



Review

Bismuth-based metal–organic frameworks and their derivatives: Opportunities and challenges



Ziwei Wang ^{a,1}, Zhuotong Zeng ^{b,1}, Han Wang ^{a,1}, Guangming Zeng ^{a,*}, Piao Xu ^{a,*}, Rong Xiao ^{b,*}, Danlian Huang ^a, Sha Chen ^a, Yangzhuo He ^a, Chengyun Zhou ^a, Min Cheng ^a, Hong Qin ^a

^a College of Environmental Science and Engineering, Hunan University and Key Laboratory of Environmental Biology and Pollution Control, Ministry of Education(Hunan University), Changsha 410082, PR China

^b Department of Dermatology, Second Xiangya Hospital, Central South University, Changsha 410011, PR China

ARTICLE INFO

Article history:

Received 6 November 2020

Accepted 4 March 2021

Available online 24 March 2021

Keywords:

Bismuth

Metal-organic frameworks

Derivatives

Structure

Application

ABSTRACT

Bismuth-based metal–organic frameworks (Bi-MOFs) and their derivatives are a class of emerging promising coordination polymers with intriguing properties and functions. However, this specific type of MOFs is still in its infancy stage, which is limited by the flexible coordination environment and low solubility of Bi(III) cation. Herein, this review aims at providing a comprehensive overview of the latest advances in Bi-MOFs and their derivatives, focusing on the three aspects: synthesis, structure, applications. The solution chemistry for Bi(III) cation is discussed firstly. The diverse structure types of Bi-MOFs with different organic ligands are fully discussed and the formation of Bi-MOFs derivatives is highlighted in the following section. Then, the applications of Bi-MOFs and their derivatives are elaborated, including catalysis, energy storage, biomedical imaging, drug delivery, fluorescence sensing, adsorption and separation. Finally, referencing these studies, the insights and perspectives are suggested in terms of future research directions. With the context of recent pioneering studies on Bi-MOFs and their derivatives, we hope to stimulate some possibilities for further development in this field.

© 2021 Elsevier B.V. All rights reserved.

Contents

1. Introduction	2
2. The solution chemistry of bismuth cation	2
3. Structure of Bi-MOFs	3
3.1. Carboxylate ligands	3
3.1.1. Ditopic carboxylate ligands	3
3.1.2. Tritopic carboxylate ligands	3
3.1.3. Tetraptopic carboxylic ligands	4
3.2. Phenolate ligands	4
4. Formation of Bi-MOFs derivatives	5
4.1. Thermal transformation	5
4.2. <i>In situ</i> electrochemical transformation	5

Abbreviations: Bi-MOFs, bismuth-based metal–organic frameworks; SBUs, secondary building units; DTTDC, dithieno[3,2-b:2',3'-d]thiophene-2,6-dicarboxylic acid; IEF, IMDEA Energy Framework; H₃BTB, 1,3,5-benzenetrisbenzoic acid; ADT, automated diffraction tomography; H₃TATB, triazine-2,4,6-triyl-tribenzoic acid; H₃BTC, benzenetricarboxylic acid; H₃BPT, biphenyl-3,4',5-tricarboxylic acid; H₄L, 3,3',5,5'-tetracarboxylic acid; H₄TBAPy, 1,3,6,8-tetrakis(p-benzoic acid)pyrene; SACs, Single-atom catalysts; ETEM, *in situ* environmental transmission electron microscopy; ECRR, electrochemical CO₂ reduction reaction; FE, faradaic efficiency; DFT, density-functional theory; LLCT, ligand-to-ligand charge transfer; LMCT, ligand-to-metal charge transfer; SCs, supercapacitors; LIBs, lithium-ion batteries; EES, electrical energy storage; PIBs, potassium-ion batteries; DCA, dichloroacetate; α -CHC, α -cyano-4-hydroxycinnamic acid; RE³⁺, trivalent rare-earth ions; Cys, cysteine; GSH, glutathione; Hcy, homocysteine; DMF, dimethylformamide; H₄TCPB, 1,2,4,5-tetrakis-(4-carboxyphenyl) benzene; TBAPy, 1,3,6,8-tetrakis(p-benzoate)-pyrene; BET, Brunauer–Emmett–Teller.

* Corresponding authors at: College of Environmental Science and Engineering, Hunan University, Changsha 410082, PR China.

E-mail addresses: zgming@hnu.edu.cn (G. Zeng), piaoxu@hnu.edu.cn (P. Xu), xiaorong65@csu.edu.cn (R. Xiao).

¹ These authors contribute equally to this article.

5. Applications	6
5.1. Catalysis	6
5.1.1. Lewis acid catalysis	6
5.1.2. Electrocatalysis	6
5.1.3. Photocatalysis	7
5.2. Electrochemical energy storage	8
5.3. Biomedical imaging and drug delivery	9
5.4. Fluorescence sensing	9
5.5. Adsorption and separation	10
6. Insights and perspectives	11
6.1. Bi-MOFs	11
6.1.1. Synthesis	11
6.1.2. Structure	12
6.1.3. Applications	13
6.2. Derivatives	13
7. Conclusion	14
Declaration of Competing Interest	14
Acknowledgments	14
References	14

1. Introduction

The past few decades have witnessed the flourishing growth of MOFs (metal organic frameworks also known as porous coordination polymers) relating to the synthesis, characterization and application [1-4]. Coordination of metals and organic units into varies of topological structures is a significant achievement in chemistry and develops a platform for constructing MOFs [5]. Their extended structures with permanent porosity are constructed by combining metal centers (secondary building units, SBUs) with organic ligands through strong bonds [6,7]. The flexible combination among various kinds of metal-containing units and organic ligands creates thousands of different MOFs [8,9]. Owing to the ultrahigh porosity and tunable functionalities, MOFs exhibit great potential in a wide range of fields, involving catalysis [10-13], sensors [14], biomedicine [15], energy storage [16,17], adsorption and separation [10,18]. Meanwhile, as the research moves on, nanomaterials derived from MOFs have also attracted widely attentions in energy and environment fields [19,20].

MOFs built from transition metal and lanthanide ions are fairly mature, which have been systematically summarized in a series of comprehensive reviews [21-23]. Researches on main group metals (In, Sn, Bi, etc.) are gained popularity recently, in which Bi metal is a fascinating representative because of lower environmental impact and manufacturing cost compared to Sn and In [24,25]. The application of bismuth and its complexes has a 250 year history, but the appearance of Bi-MOFs is more recent, which was pioneered and emphasized by the group of Norbert Stock in 2012 [26,27]. The development of bismuth-based reticular chemistry results in the realization of architecturally stable and permanently porous Bi-MOFs, and some of them exhibit great potential in catalysis [28,29], sensing [30,31] and biomedicine [32,33]. Additionally, diverse bismuth-based nanostructures derived from Bi-MOFs through thermal transformation and *in situ* electrochemical transformation have been widely used as electrocatalysts [34-38], photocatalysts [39,40] and electrode materials [41-43]. Some important advances in Bi-MOFs and their derivatives are shown in Fig. 1. Since a number of Bi-MOFs and their derivatives have reported very recently, an overview of this challengeable research field to provide insight understanding is highly desirable.

In this review we will illustrate an overall scope of the Bi-MOFs and their derivates, while the bismuth compounds (limited porosity) are outside the scope of this review. To highlight the unique advantages of Bi-MOFs and their derivatives, we first delineate the essential features and coordination chemistry of Bi(III) cations.

Subsequently, we comprehensively review the works published from the breakthrough of 2012 to the latest term of 2020, covering the synthetic chemistry and structure types. Promising applications of Bi-MOFs with diverse structures, such as catalysis, energy storage, biomedical imaging, drug nanocarriers, fluorescence sensing, adsorption and separation, are then presented. Afterwards, a perspective with remaining challenges and opportunities, including synthesis, characterization, application, is discussed in the basis of chemistry and materials science.

2. The solution chemistry of bismuth cation

Up to now, more than 70,000 MOFs have been reported and diverse metal cations are utilized to build up MOFs, including monovalent, divalent, trivalent and tetravalent cations [44]. Undoubtedly, transition metal elements are predominant in reticular chemistry of MOFs, followed by rare earth cations and other main group cation [45]. Although some breakthroughs have been made in Bi-based reticular chemistry, Bi-MOFs are still understudied. To highlight the distinct advantages of Bi-MOFs, we herein begin with a brief introduction of the solution chemistry of Bi(III) cations.

Bismuth, a nontoxic and noncarcinogenic metal with $4f^{14}5d^{10}6s^26p^3$ ground-state electron configuration, usually exhibits an oxidation state of +3 in most complexes [46]. Although Bi (III) is an attractive metal cation, its use in elaborating MOFs remains the great challenge. Such a situation may result from the special chemistry of Bi(III). The three 6p electrons are in charge of bond formation during coordination, which leads to a stereoactive lone-pair of $6s^2$ electrons [47]. Given this flexible coordination geometry, the Bi(III) cation tends to form dense nonporous or layer materials [48]. Therefore, the Bi(III)-based inorganic-organic framework materials are often reported with poor porosity.

According to Pearson's hard-soft acid-base theory, Bi(III) cation is borderline acid and possesses a much affinity for multiple negatively charged linkers based on O atoms [49]. Therefore, anions of poly-carboxylates are ideal ligands towards Bi (III) cation due to the strong chelation effect [50,51]. Moreover, Bi(III) is easily hydrolysis ($pK_a = 1.5$) and has a bigger ionic radius (1.17 Å) with low electronegativity and strong polarizing ability [52]. Such a nature of the cation is adverse to MOFs synthesis reaction, leading to the uncontrollable and irregular nucleation, and thereby causing the formation of microcrystalline coordination polymer or mixture with various phases and clusters [53]. As a consequence, control over the reactivity of Bi(III)

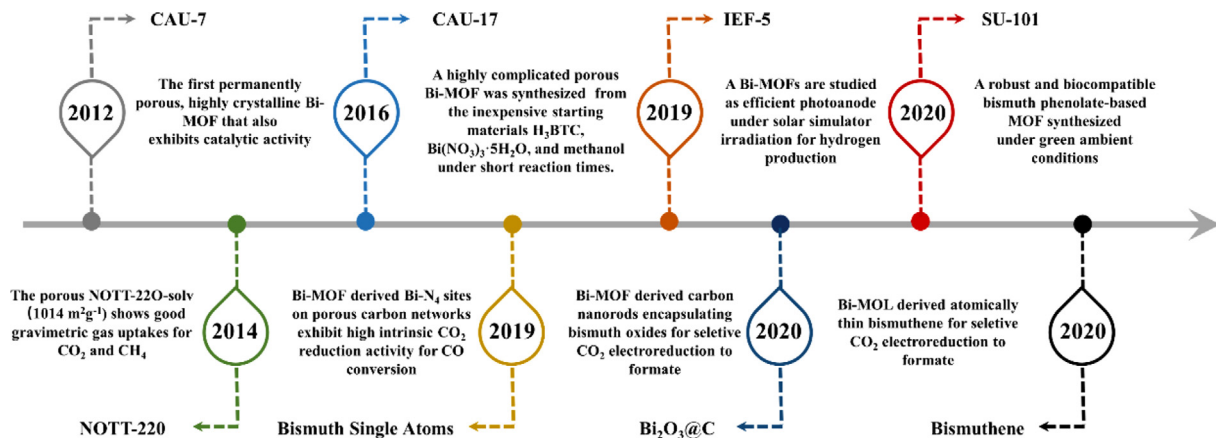


Fig. 1. Some important advances in Bi-MOFs and their derivatives.

by selecting solvents, ion concentration, reaction temperature and time is one of the key factors in Bi-MOF synthesis. Sometimes, the additives such as HF or monocarboxylate species can either be nonnegligible as they could slow down MOF crystal growth and lead to larger single crystals [54,55].

3. Structure of Bi-MOFs

A number of organic-inorganic coordination compounds based on Bi(III) cation have been reported so far, but Bi-MOFs with connected frameworks and accessible porosity are relatively limited. Given that the structural diversity mainly depended on the definite interconnection between Bi-containing units and multicomponent organic ligands, this section will encompass all Bi-MOFs reported up to date which were classified on the basis of utilized organic ligands, namely carboxylates and phenolates.

3.1. Carboxylate ligands

3.1.1. Ditopic carboxylate ligands

Carboxylate ligands are easily synthesized or commercially available, thereby they are primarily applied to fabricate Bi-MOFs. Among them, linear dicarboxylate ligands are diffusely utilized to fabricate high valence cations (+III, +IV...) based MOFs, but only a few of Bi-MOFs with limited porosity have been described. Among ditopic carboxylate ligands, pyridine dicarboxylic acid has attracted the most attention [56–58]. A representative example is Bi(pydc)₂·(H₃O⁺)_{0.83}, a unique 2-D sheet structure with the **Kagome'** topology [56]. In this compound, bismuth centers were composed of O and N atoms from the four pydc²⁻ ligands. Each bismuth center connected four pydc²⁻ ligands and extended along the crystallographic ab plane of the rhombohedral structure, resulting in a typical **Kagome'** topology with three- and six-membered rings with both crystallographic diameter of 8.367 Å and 16.716 Å. Notably, the structure of this compound tended to collapse when it was filtered from the mother liquor because of the existence of water molecules in its channels.

Heterocyclic dicarboxylate ligand is also used in the design and construction of Bi-MOFs. Alba et al. [28] utilized dithieno[3,2-b:2',3'-d]thiophene-2,6-dicarboxylic acid (DTTDC) as the ligand to synthesize IEF-5 (IEF stands for IMDEA Energy Framework). In IEF, three linearly arranged bismuth atoms were coordinated to twelve carboxylates from twelve DTTDC linkers to yield the inorganic SBUs. Each SBU linked six neighboring ones with pairs of parallel linkers to form a **pcu** network. In this framework, water and DMF molecules located between two interpenetrated networks. A poor

BET surface area of about 30 m² g⁻¹ was determined, which was in alignment with the presence of dimethylammonium cations in the pores.

3.1.2. Tritopic carboxylate ligands

In the limited Bi-MOFs with permanently porous, the versatility of tritopic carboxylate ligands as Bi-MOFs building blocks are well investigated by Norbert Stock's group [27,48]. 1,3,5-benzenetrisbenzoic acid (H₃BTB) was employed in Bi-MOF construction firstly. The structure of Bi(BTB) denoted CAU-7 was determined by single-crystal automated diffraction tomography (ADT) (Fig. 2a). CAU-7 crystallized in the space group *Pb2_1a* and was a trigonal prismatic particle composed of three individuals sharing the [001] axis. In this framework, each Bi(III) cation was connected to nine-fold oxygen atoms of H₃BTB ligands to form linear face sharing BiO₉ polyhedra along the [001] axis. The BTB³⁻ linkers connected the chains to construct the wall of a marked hexagonal network with a diameter of 10 Å and one-dimensional channels. CAU-7 was of great thermal stability (stable up to 380 °C) and high porosity (BET surface area, 1150 m² g⁻¹, and pore volume, 0.43 cm³ g⁻¹). Inspired by this work, Norbert Stock et al. [59] then synthesized CAU-7-TATB (also denoted as CAU-35) with nearly the same structure as CAU-7 by using triazine-2,4,6-triyltribenzoic acid (H₃TATB) as the ligand. In CAU-35, a highly condensed chain was built up from linear inorganic building unit (IBU) with BiO₇-polyhedra sharing the formula of {Bi₂O_{6.5}}. The IBUs contained two modes of coordinated oxygen atoms: one was connected to four Bi(III) cation (μ_4 -O²⁻ ion) and another was coordinated by three Bi(III) cation (μ_3 -OH⁻ ion). With these binding modes, the substructure of a honeycomb net with an additional ligand inside the distorted pores was formed.

With H₃BTC, the same group later described the synthesis of CAU-17. The structure and connectivity of CAU-17 exhibited unprecedented complexity among MOFs structures (Fig. 2b). CAU-17 had three crystallographically independent rods and each rod was composed of three independent Bi(III) cation. Each Bi(III) cation was nine-coordinated by O atoms, in which eight O atoms were originated from carboxylate groups while the ninth was a terminal water molecule. The rods of distorted face-sharing octahedra were linked with four other rods through the ligands to construct a **htb** net in the ab-plane. Interestingly, there were five crystallographically independent channels in each single net with diameters of 9.6, 9.6, 3.6, 3.6, and 3.4 Å, respectively (Fig. 2c). Soon after, Zou et al. [60] synthesized SU-100 by using flexible biphenyl-3,4',5-tricarboxylic acid (H₃BPT) taking after the preparation of CAU-17. For SU-100, the inorganic nodes were based on a Bi₂O₁₂ dimer, where each Bi(III) cation was seven-coordinated by

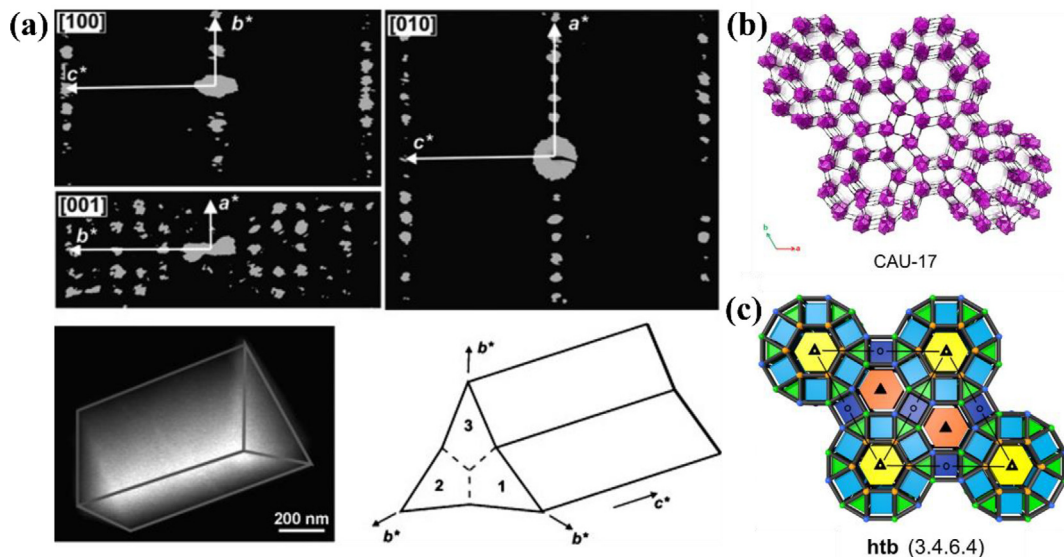


Fig. 2. (a) Reconstructed three-dimensional diffraction space of CAU-7 projected along the main directions (top), a rod tilted to expose the triangular base (bottom left), and a sketch of the trilling arrangement (bottom right). (b) Crystal structure of CAU-17. Bismuthoxygen polyhedra are colored purple. (c) The **htb** net is overlaid with symmetry elements found in CAU-17. Unlike the standard **htb** net, CAU-17 has three symmetry independent rods (orange, green, and blue nodes), two hexagonal channels (orange and yellow hexagons), and two independent rectangular channels (light and dark blue rectangles) and one type of triangular channel (green triangle). Reprinted with permission from Ref. [27,48]. Copyright 2012, WILEY-VCH and Copyright 2016, American Chemical Society.

O atoms and two of the bismuth atoms were bridged by two oxygen atoms in an edge-sharing manner. In the framework of SU-100, six carboxylate groups coordinated with a Bi_2O_{12} dimer, constructing a net with **esg** topology. It was clear that the dimer took an important part in the changes of both unit cell volume and solvent accessible void volume inside the framework, thereby presenting solvent dependent flexibility.

3.1.3. Tetratopic carboxylic ligands

Tetracarboxylate ligands are favorable linkers for fabricating Bi-MOFs due to rich coordination patterns and large space steric hindrance, which could efficiently avoid framework interpenetration. In 2014, Mathew Savage et al. [61] used 3,3',5,5'-tetracarboxylic acid (H_4L) to synthesize $[\text{Bi}_2(\text{C}_{16}\text{H}_6\text{O}_8)_{1.5}(\text{H}_2\text{O})_2]\text{(DMF)}_{3.5}\text{(H}_2\text{O})_3$ with non-interpenetrated structure, denoted as NOTT-220. A finite SBU (binuclear Bi_2O_{14} clusters) was observed in this framework. Each $\text{Bi}(\text{III})$ cation was connected to three different H_4L ligands by three carboxylate groups and both $\text{Bi}(\text{III})$ cation shared three carboxylate oxygen atoms from corresponding groups. It should be noted that the cluster could change from a to b phase according to the different coordination modes of two water molecules. Each Bi_2O_{14} cluster was connected to six L^{-4} ligands considered as two 3-c vertices, thus leading to the construction of a novel topology with 3,6-connected framework structure. The framework was highly porous and contained three interconnected pore channels with inner diameters of 8.3, 5.3 and 3.2 Å, respectively.

Among all tetratopic carboxylic ligands, 1,3,6,8-tetrakis(p-benzoic acid)pyrene (H_4TBAPy) is quiet commonly applied for the fabrication of MOFs based on transition elements [62–64], main group elements [65] and actinide elements [66]. As shown in Fig. 3a and 3d, this ligand contains two types of coordination modes: $\mu_8\text{-}\eta^1\eta^1\eta^1\eta^1\eta^1\eta^1\eta^1\eta^1$ and $\mu_4\text{-}\eta^2\eta^2\eta^2\eta^2$. For the former, Bi-NU-901 has been described by Farha's group [33]. The framework of Bi-NU-901 had a **scu** topology, parallels with that of Zr-NU-901, consisting of 8-connected $[\text{Bi}_6\text{O}_4(\text{OH})_4(\text{NO}_3)_6(\text{H}_2\text{O})]$ (H_2O) octahedral clusters (Fig. 3b, c). The framework involved stacked diamond-shaped 1D channels with the BET surface area

of $320 \text{ m}^2 \text{ g}^{-1}$. Meantime, two kinds of stable bismuth-organic framework with $\mu_4\text{-}\eta^2\eta^2\eta^2\eta^2$ coordination mode were constructed from H_4TBAPy ligands, denoted Bi-TBAPy-1 [30] and Bi-TBAPy-2 [29], separately. Bi-TBAPy-1 and Bi-TBAPy-2 were two stable bismuth-organic frameworks formed by a parent-framework node of a BiO_8 double-cap triangular prism, where each $\text{Bi}(\text{III})$ cation was connected to eight O atoms from four different TBAPy ligands (Fig. 3e). In Bi-TATBy-1, the 3D structure could be described as a square layer stacked by H_4TBAPy , resulting in 4-connected **sra** uninodal topology (Fig. 3f). The framework of Bi-TATBy-1 involved large cages with a channel of $16.3 \text{ \AA} \times 11.6 \text{ \AA}$ in size. In Bi-TATBy-2, each TBAPy $^{+4}$ ligand was bridged by four IBUs, leading to a structure with two shapes of 1D channels along the axis: rhomboid and quadrilateral (Fig. 3g). The length on both sides of two different windows were 7.37 \AA and 11.65 \AA , respectively. From the N_2 adsorption isotherm at 77 K , it exhibited permanent porosity with a BET area of $594 \text{ m}^2 \text{ g}^{-1}$.

3.2. Phenolate ligands

This topic is recently addressed by a series of research [67]. Compared with carboxylate based MOFs, most of phenolate-based MOFs exhibit higher chemical stability, possibly as a result of the higher pK_a of the phenolate groups, generating stronger chelation ability [68]. The pioneering systematic study of the phenolate ligands-based Bi-MOFs construction was performed by using ellagic acid as linkers [69]. This crystalline phenolate-based Bi-MOFs was SU-101 ($\text{Bi}_2\text{O}(\text{H}_2\text{O})_2(\text{C}_{14}\text{H}_2\text{O}_8)\text{nH}_2\text{O}$), reported in 2020 by Horcajada et al., via water-based room temperature synthesis. The structure of SU-101 was composed of rod-shaped SBUs linked by ellaglate ligands in the ab-plane, resulting in a uninodal 7-coordinated net **svd**. In the SBUs, each Bi atom was coordinated by six oxygen atoms, three from phenolates groups, two from μ_4 -oxygens and a bonded water molecule. The 3D framework provided one-dimensional pores with accessible diameters of $6\text{--}7 \text{ \AA}$ and showed a BET surface area of $412 \text{ m}^2 \text{ g}^{-1}$. SU-101 was robust and displayed highly chemical stability in aqueous

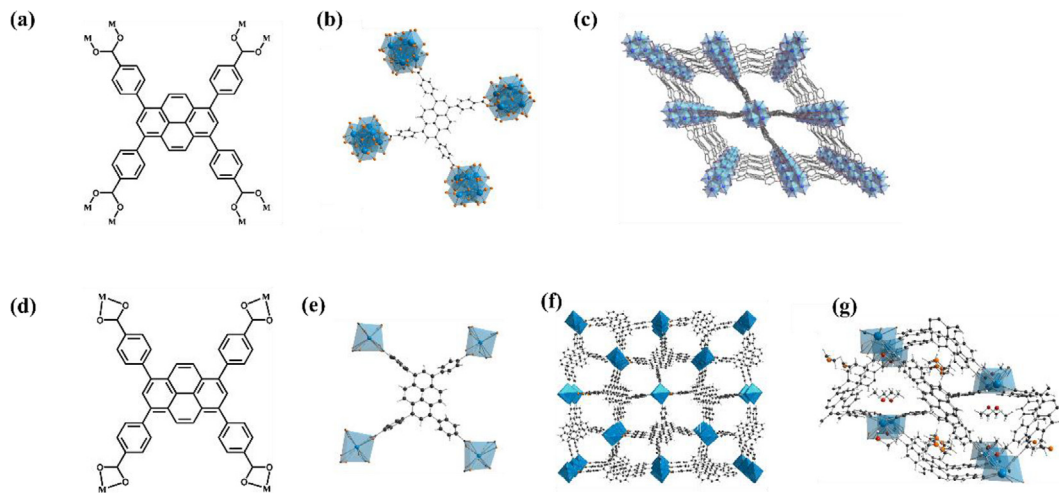


Fig. 3. (a) Coordination modes of H₄TBAPy ligand: $\mu_8\text{-}\eta^1\eta^1\eta^1\eta^1\eta^1\eta^1\eta^1$; (b) the coordination mode of the TBAPy moiety in Bi-NU-901; (c) crystal structure of Bi-NU-901; (d) coordination modes of H₄TBAPy ligand: $\mu_4\text{-}\eta^2\eta^2\eta^2\eta^2\eta^2$; (e) the coordination mode of the TBAPy moiety in Bi-TBAPy-1 and Bi-TBAPy-2; (f) crystal structure of Bi-TBAPy-1; (g) crystal structure of Bi-TBAPy-2. Reprinted with permission from Ref. [29,30,33]. Copyright 2019, Elsevier and American Chemical Society.

conditions (pH = 2–14, hydrothermal and heated organic solvents). Discovery of SU-101 stimulates the studies of Bi-MOFs in a green and economic manner, paving the ways for large-scale of synthesis and development of new Bi-MOFs structure.

4. Formation of Bi-MOFs derivatives

MOFs are constructed by self-assemblies of metal ions and organic linkers, which possess high surface area, tailoriable structures and well-defined metal centers. These properties make MOFs scaffold a variable platform to fabricate versatile micro-/nanomaterials [8,20,70]. MOFs derivatives, inheriting frameworks and strengths from parent MOFs, not only afford controllable composition and morphology but also realize the integration of multiple functions [19]. In this section, we summarize the synthetic strategies utilized to construct Bi-MOFs derivatives, including thermal transformation and *in situ* electrochemical transformation, which highlight the exploration in composition and morphology control.

4.1. Thermal transformation

The self-templating method is a common strategy to preserve the original morphologies and generate the corresponding metal-/carbon or metal oxides/carbon hybrids via a direct pyrolysis of MOFs precursors [34,42,71,72]. To prepare metal/carbon hybrids, the Bi-MOFs are generally polysized under the inert atmosphere (e.g. N₂, Ar). Due to the well-defined and localized interaction between metal units and organic ligands in the nanoscale, the derivatives usually possess monodisperse metal nanoparticles in organic matrix. For instance, an one-step thermal treatment of Bi-MOFs based on benzenetricarboxylic acid in Ar atmosphere at 700 °C generated the dispersed Bi nanoparticle encapsulated in the carbon film (Fig. 4a) [42]. Moreover, nanocomposites of metal oxides and carbon could be synthesized via thermal transformation of MOFs in air [73]. For instance, Xia et al. [35] adopted a two-step pyrolysis method to synthesize carbon nanorods encapsulating Bi₂O₃ (Fig. 4b). In this regard, CAU-17 nanorods were carbonized in Ar atmosphere followed by an oxidation process at 200 °C.

The direct pyrolysis of MOFs with the assistance of secondary heteroatom sources can endow the resultant carbons with doped heteroatoms [25]. As a very recently report, Bi nanoparticles

encapsulated in N-doped carbon nanocages were prepared from novel 2D Bi-MOFs precursors under Ar atmosphere using the melamine as the nitrogen source [43]. When Bi nanoparticles were exposed to the N-dopants in the carbon framework, the N-dopants would anchor the Bi atoms and prevent their agglomeration. Furthermore, Zhang and co-workers [34] adopted Bi-BTC as template and dicyandiamide as nitrogen source to synthesize Bi single-atom catalysts by *in situ* thermal atomization of Bi nanoparticles (see Fig. 4c). In this synthesis process, NH₃ gas originated from dicyandiamide could effectively assist the isolated atomization of Bi nanoparticles and downsize the metal sizes. Then, isolated Bi atoms were trapped by the N-dopants in carbon networks and supported Bi SACs with Bi-N₄ structure were achieved.

Apart from metal/carbon or metal oxides, diverse metal-based functional materials such as carbonate-hydroxides [39], telluride [74], sulfides [75,76] and oxyhalides [40,77] could be fabricated by tuning the MOFs-based composites. Tang et al. [76] synthesized Bi₂S₃ nanorods via the direct pyrolysis of the mixture of Bi-BTC and sulfur powder and further found that mixing Bi-BTC with proper amounts of H₃BTC before calcination could finely tune carbon content. Our group also designed nanosized Bi₂O₂CO₃/porous g-C₃N₄ heterojunctions via one-shot pyrolysis of CAU-17/melamine precursors [39]. Only the diffraction peaks of pure monoclinic phase Bi₂O₃ was detected in the XRD pattern after the calcination of CAU-17. With the addition of melamine, an abundant CO₂ atmosphere was formed during calcination, promoting the construction from Bi-O bonds of Bi₂O₃ to Bi-O-C bonds in Bi₂O₂CO₃. Furthermore, the porous bismuth oxyhalide could be obtained through Bi-MOFs halogenation with halogen sources (NH₄X, X = Cl, Br, I, and CTAB) followed by a calcination treatment [40,77]. Compared to traditional inorganic precursors, Bi-MOFs provide a perfect platform to simply fabricate various functional materials in well-designed manners.

4.2. *In situ* electrochemical transformation

Besides, *in situ* electrochemical transformation represents another facile way to obtain Bi-MOFs derivatives with interesting nanostructures. The possible transformation mechanism is speculated that the surface Bi(III) species of Bi-MOFs are rapidly reduced to Bi atoms during the *in situ* electrochemical reduction.

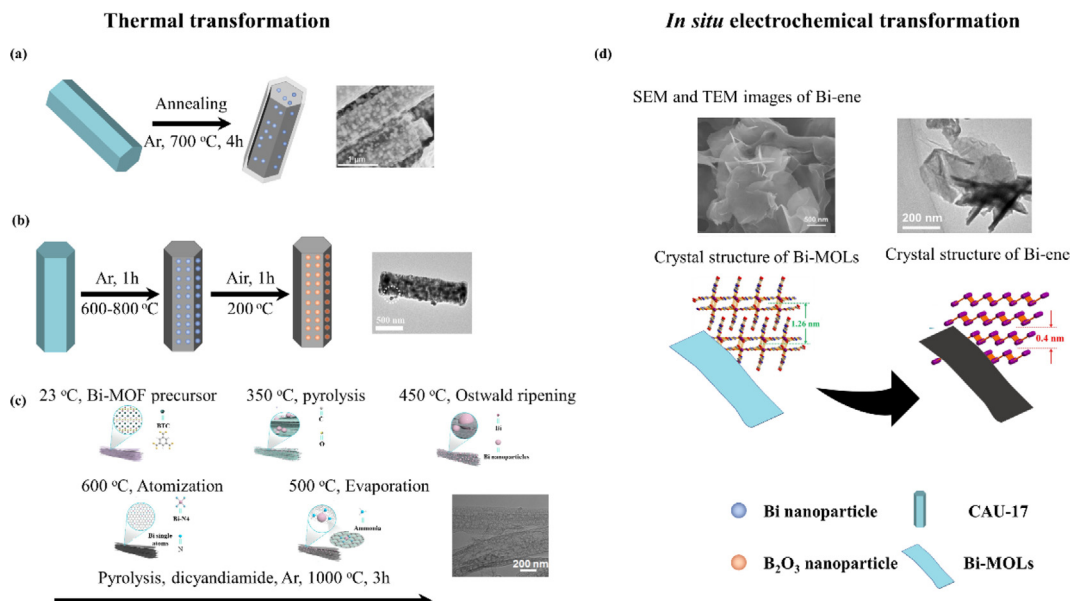


Fig. 4. Compositional and morphological control of Bi-MOFs derived materials. (a) synthesis of ultrathin carbon film@carbon nanorods@Bi nanoparticle and its TEM image; (b) synthesis of $\text{Bi}_2\text{O}_3@\text{C}$ catalyst and its TEM image; (c) scheme of the transformation from Bi-MOF to single Bi atom and its TEM image; (d) the *in situ* electroreduction-derived transformation from Bi-MOLs to Bi-ene. Reprinted with permission from Ref. [34,35,38,42]. Copyright 2019, Elsevier Copyright 2020, American Chemical Society and WILEY-VCH.

Meanwhile, the reduced Bi atoms and internal Bi(III) species are inclined to migrate due to the gradual loss of organic linkers. As a result, the migrated Bi atoms and the dissociated linkers work as soft templates to shape a final morphology. A case in this point is the *in situ* electrochemical transformation from bismuth-based metal organic layers (Bi-MOLs) to atomically ultrathin bismuthine, which exhibited excellent catalytic performance and cycle stability for ECCR (Fig. 4d) [38]. Similarly, Yao et al. [37] and Yang et al. [36] also developed this strategy for the preparation of fragmented bismuth nanoparticles and leaf bismuth nanosheets, respectively. Moreover, Gu's group [78] successfully prepared $\text{Bi}_2\text{O}_2\text{CO}_3$ by *in situ* electrochemical transformation of bismuth-carboxylate MOFs (Bi-BTB, Bi-TATB) in HCO_3^- solution.

5. Applications

5.1. Catalysis

MOFs and their derivatives have exhibited great potential in catalysis, which is one of the earliest proposed applications and has been discussed in several comprehensive reviews [79–81]. The diversified and tailororable structures as well as porosity place them at frontier than conventional catalysts [11,12,82,83]. Bi-based materials are promising candidates due to their excellent activity and environmentally benign nature. Herein, the catalytic application is elaborated from three types of catalytic reactions: Lewis acid catalysis, electrolysis and photocatalysis.

5.1.1. Lewis acid catalysis

CAU-17, which has accessible edge-sharing helical BiO_9 polyhedra, is a representative example of the concept of Lewis acid Bi-MOFs [48,84]. Each BiO_9 polyhedra in the framework of CAU-17 contains an oxygen atom from the terminal water molecule. Through identical activating reaction, the coordinate water molecular could be easily removed, creating Bi(III) Lewis acid sites available to a reactant. The properties of Lewis acidity were tested in the ring-opening of styrene oxide to 2-methoxy-2-phenylethanol [84]. CAU-17 exhibited complete conversion with 100% regioselectivity to 2-methoxy-2-phenylethanol, which convincingly proved the existence of hard Lewis acid centers. Compared to CAU-17, CAU-7 displayed a much low catalytic activity in this reaction. This could be ascribed to acid sites of moderate strength in CAU-7, while the structure showed no evidence for open metal sites or catalytic –OH groups. Such acid sites were also proved in the solvent-free hydroxymethylation of 2-methylfuran to 5-methylfurfurylalcohol [27]. Among CAU-7, UiO-66 and MIL-53 (Ga), CAU-7 showed the best catalytic activity with 75% yield at 90% conversion. Although UiO-66 had more active Lewis acid sites, the mild Lewis acid sites and hydrophobic nature of CAU-7 could restrain the further consecutive condensation reactions and the production of a tarry resin.

tivity to 2-methoxy-2-phenylethanol, which convincingly proved the existence of hard Lewis acid centers. Compared to CAU-17, CAU-7 displayed a much low catalytic activity in this reaction. This could be ascribed to acid sites of moderate strength in CAU-7, while the structure showed no evidence for open metal sites or catalytic –OH groups. Such acid sites were also proved in the solvent-free hydroxymethylation of 2-methylfuran to 5-methylfurfurylalcohol [27]. Among CAU-7, UiO-66 and MIL-53 (Ga), CAU-7 showed the best catalytic activity with 75% yield at 90% conversion. Although UiO-66 had more active Lewis acid sites, the mild Lewis acid sites and hydrophobic nature of CAU-7 could restrain the further consecutive condensation reactions and the production of a tarry resin.

5.1.2. Electrocatalysis

Electrocatalysis is one of the most important application fields of MOFs and their derivatives [34,80,81,85,86]. Considering the rising global atmospheric CO_2 concentration, the electrochemical CO_2 reduction reaction (ECRR) draws growing attention recently [87,88]. Main group metals such as In, Sn, Bi, Tl exhibit extraordinary potential in this field due to the selective production of formate or CO. Among these metals, bismuth attracts widely interest due to its nontoxicity, environmental benignity and relatively low cost [34,85,89]. Besides, Bi exhibits larger overpotential for the competitive hydrogen evolution reaction, which is beneficial to selectively accelerate CO_2 reduction reaction [24]. To efficiently evaluate the electrocatalysis CO_2 reduction performance of an electrocatalyst, key factors including onset potential, faradaic efficiency (FE), partial current density and stability are usually adopted [18,90].

With respect to the Bi-MOFs derivatives, metallic bismuth-based materials have drawn tremendous attention as one of promising electrocatalysts owing to high selectivity and faradaic efficiency. For example, Hu's group [91] directly utilized Bi-BTB as pre-catalyst to fabricate a novel electrocatalyst *in situ* under CO_2 reduction reaction conditions. The catalysts were consisted of Bi nanoparticles embedded into a porous carbon matrix. Electrochemical experiments revealed that the catalysts enabled selective

CO_2 reduction reaction to formate with peak FE of 95(3)% at an overpotential of 770 mV. Due to the low load of Bi atoms, the Bi-BTB derivatives reached the best mass activity among investigated Bi-based catalysts (Fig. 5a). Modulating the chemical composition and morphology of Bi-MOFs derivatives distinctly influence the inherent catalytic performance. Wang et al. [92] designed a chloroplast-like core-shell Bi@ Bi_2O_3 by using Bi-MOFs (CAU-17) as precursors. This core-shell Bi@ Bi_2O_3 catalyst exhibited a remarkable FE towards formate production (nearly 100%), a current density of $\sim 22.9 \text{ mA cm}^{-2}$ at -1.0 V and catalysis stability ($>72 \text{ h}$). More recently, single-atom catalysts (SACs), the isolated metal atoms embedded on a specific support, display better catalytic activity, stability and selectivity compared to nanoparticles [93]. Following this guiding principle, Li's group [34] reported that single Bi-N₄ sites on N-doped carbon supports derived from Bi-BTC exhibited excellent activity towards CO_2 reduction reaction (Fig. 5b). The prepared derivatives efficiently enabled ECRR to CO with a FE up to 97%, a moderate partial current density of 5.1 mA cm^{-2} and stability for 4 h at potential of -0.5 V versus reversible hydrogen electrode. Importantly, density-functional theory (DFT) calculations displayed that isolated Bi atoms on porous carbon matrix effectively promoted the formation of *COOH intermediates due to the lower Gibbs free energy (Fig. 5c).

The flow cells represent a promising technology due to the practical commercialization of the ECRR to C1 product requiring the FE of $>95\%$, the current density of $>200 \text{ mA cm}^{-2}$ and the catalysts stability of $>1000 \text{ h}$ [94]. Carbon nanorods encapsulating Bi_2O_3 [35] exhibited high activity for CO_2 reduction reaction to formate. When evaluated in the flow-cell configuration, this electrocatalyst maintained a high current density of over 200 mA cm^{-2} at -1.1 V vs. RHE and excellent formate FE of $>93\%$ over a broad potential (Fig. 5d). Recently, two-dimension bismuth materials recently have aroused growing attentions due to the large charge carrier mobility and high intrinsic ECRR activity [95]. Cao et al. [38] successfully in-situ prepared atomically thin bismuthene by using Bi-based metal-organic layers as pre-catalyst. The resulting material displayed excellent catalytic activity for the CO_2 electroreduction to formate, especially in the flow-cell configuration

(Fig. 5e). The current density exceeded 300 mA cm^{-2} in a self-designed flow cell and the FE achieved nearly 100% in a typical H-type electrochemical cell, which outperformed the performance of most reported catalysts (Fig. 5f).

Bi-MOFs also exhibit promising potential in the field of electrochemical CO_2 reduction. It has been reported that a layered MOF fabricated from tritopic linkers, similar to CAU-17, displayed good activity and selectivity for the CO_2 reduction to HCOOH formation [96]. Electrocatalyst materials showed the 2D Bi-MOF delivered partial current density of $41 \text{ mA mg}_{\text{Bi}}^{-1}$ and a significant formate FE of 92.2% at an overpotential of 0.65 V with impressive stability $>30 \text{ h}$. Although Bi-MOFs based ECCR has been successfully investigated in this work, the abnormal structure stability of Bi-MOF during ECRR process is not clear. Further explorations on the reaction process and mechanism for the conversion of from Bi(III) citation to Bi metallic in Bi-MOFs by using *in situ* characterizations and resolved spectroscopy are recommended, such as *in situ* Raman spectroscopy and *in situ* environmental transmission electron microscopy.

5.1.3. Photocatalysis

Photocatalysis, a technology to convert solar energy into renewable energy, is considered as a promising strategy to alleviate the increasing environmental pollution and energy shortage [97-100]. In line with the excellent performance of Bi(III)-containing inorganic semiconductors in photocatalysis, Bi(III)-based MOFs show great potential in this field [101,102]. With respect to pollutants degradation, Bi-mna (2-mercaptopurine acid) as photocatalyst was first applied for Rhodamine B (RhB) decomposition and exhibited high photocatalytic activity with 95% degradation efficiency in 2 h [103]. A reaction mechanism was proposed that photo-induced electrons firstly transferred from the S atoms to the O atoms of the nonadjacent pyridine ring, and then the Bi atoms acted as an electron shuttle pathway for charge transfer between the ligands. Such a ligand-to-ligand charge transfer (LLCT) is distinguished from the widely accepted ligand-to-metal charge transfer (LMCT) mechanism in most of MOFs, which could be ascribed to the closed shell nature of Bi(III) ($d^{10} s^2$).

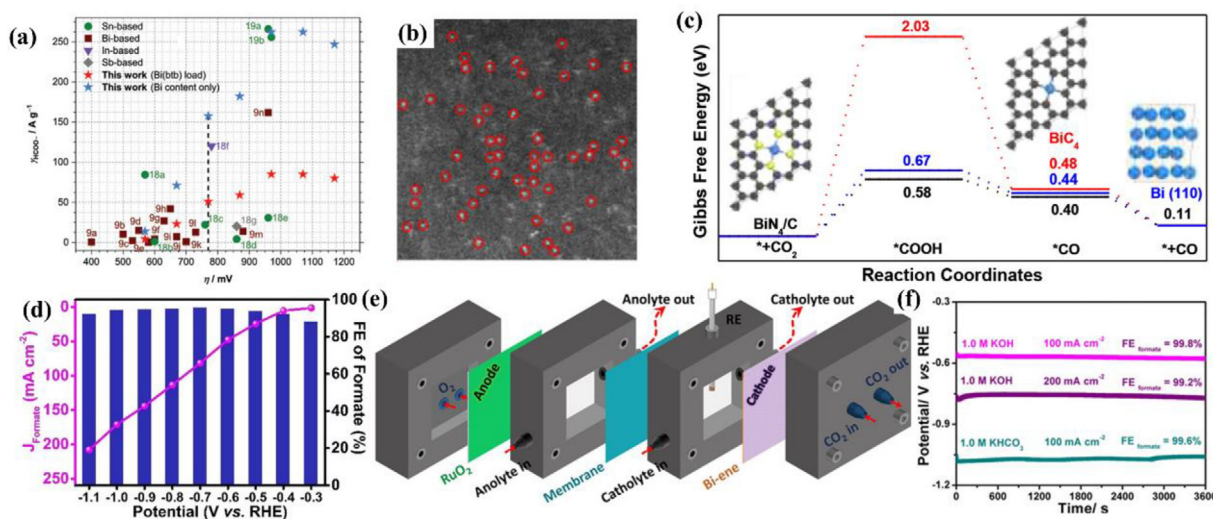


Fig. 5. Electrochemical CO_2 reduction reaction of Bi-MOFs and their derivatives. (a) Mass activity calculated for the production of formate ($\gamma_{\text{HCOO}-}$) over the mass load of Bi (btb) and of Bi in comparison with the state-of-the-art main-group metal-based eCO₂RR catalysts, referring their mass activity to the metal content. The overpotential corresponding to the applied potential $-0.97 \text{ V}_{\text{RHE}}$, at which the highest Faradaic efficiency for formate was obtained, is marked with a vertical dashed line. Reprinted with permission from Ref. [34,35,91]. (b and c) single Bi atoms derived from Bi-BTC for electrolysis CO_2 reduction: morphology illustrations of Bi single atoms, FE efficiency and calculated Gibbs free energy diagrams for CO_2 electroreduction to CO on different catalysts. (d) Faradaic efficiency and partial current density of formate for $\text{Bi}_2\text{O}_3@\text{C}-800$ in all potentials range. (e and f) Electrocatalytic CO₂RR performance of Bi-ene in a flow cell and chronopotentiometric curves at 100 and 200 mA cm^{-2} in 1.0 M KHCO_3 and KOH . Reprinted with permission from Ref. [34,35,91]. Copyright 2019, American Chemical Society and copyright 2020, WILEY-VCH.

The use of Bi-MOFs as photocatalysts or photoelectricity catalysts for water splitting (hydrogen/oxygen evolution) is one of the promising reactions in catalysis [8,104–107]. In this process, oxygen evolution is recognized as the bottleneck of photocatalytic water splitting due to the complex redox reaction involving four electrons. Bi-BTC, a MOF based on bismuth(III) and H₃T₂CO₃ with topology structure composed of centrosymmetric dimeric {Bi₂O₁₄} units, exhibited excellent photocatalytic performance towards O₂ generation [108]. Under UV–Vis illumination, the O₂ evolution rate was up to 880 μL h⁻¹. However, the framework of Bi-BTC was collapse after photocatalysis. In order to enhance the stability against photo-corrosion processes and boost electron-hole separation, an efficient way is to use ligands with an electron-rich rigid core, thereby endowing hole-transport ability to directly build MOFs. In 2019, IEF-5 [28], a bismuth-based MOF based on DTTDC, was reported and showed great photoelectrochemical performance for hydrogen production. And the H₂ production over IEF-5 reached to 2.35 μmol cm⁻² in 1 h (Fig. 6a). Solid state photoluminescence measurements and transient absorption spectrum were applied to explore the first step of charge separation on IEF-5, proving the energy transfer process of increased triplet excitons (³IEF-5*), in which the heavy atom effect of bismuth(III) citation and the existence of sulfur elements as well as thiophene moieties in the framework synergistically promoted intersystem crossing process efficiency (Fig. 6b, c). Subsequently, the photogenerated holes interacted with the hole scavenger (SO₃²⁻) and injected charge into the structure, resulting in the construction of the MOF radical anion (IEF-5⁻). It should be pointed out that this intermediate state played a critical role for the enhancement IEF-5 photoelectrochemical activity, as the oxidation reaction could be conducted on a singlet excited state (¹IEF-5*) or ³IEF-5*. The H₂ evolution reaction was performed on cathode (Pt) via the photoinduced electrons transferred from IEF-5. The closed redox cycle was indicated in Fig. 6d.

Benefiting from high stability, abundant active sites and excellent electron-hole separation, an emerging application of Bi-MOFs derivatives is photodegradation of organic pollutants [8,72,109]. For example, the Bi₂O₂CO₃/porous g-C₃N₄ derived from CAU-17/

melamine precursors manifested better photocatalytic performance than most of Bi₂O₂CO₃-based, MOF-derived and g-C₃N₄-based (melamine) photocatalysts for the photodegradation of sulfamethazine and tetracycline [39]. The prominent activity could be ascribed to the unique structural features of Bi₂O₂CO₃/porous g-C₃N₄ nanocomposites, involving nanosized heterojunction, intimate contact at the interface and doped N atoms escaping from g-C₃N₄ to Bi₂O₂CO₃, accelerating the interfacial charge transfer process and simultaneously providing a charge transport chain for the subsequent oxidation of O₂⁻ by holes (Fig. 6e, f). Moreover, a hierarchical BiOBr/Bi₂₄O₃₁Br₁₀ heterojunction starting from Bi-BTC was fabricated via a one-step bromination-annealing process [77]. These photocatalysts exhibited excellent pH adaptability, good reusability and well activity. After illumination for 60 min, the RhB removal efficiency was reached 92.4%.

5.2. Electrochemical energy storage

The energy storage technologies, including batteries and supercapacitors (SCs), are the most promising devices for sustainable development [110]. SCs, also known as electrochemical double-layer capacitors, usually employ carbon materials with porosity and high specific surface area as negative electrodes. However, they are limited by low specific capacitance and poor energy density. In this regard, metal oxides derived from MOFs have attracted increasing attention due to their intrinsic properties. For instance, Yu et al. [73] displayed the synthesis of Bi₂O₃ microrods with a carbon coat through simple heat treatment of CAU-17 and explored the Bi₂O₃/C as negative electrode materials for supercapacitors (Fig. 7a and b). The as-obtained Bi₂O₃/C exhibited a specific capacity with 1378 C g⁻¹ at 0.5 A g⁻¹ and revealed long-term retention of 93% after 4000 cycles. Overall, carbon layers efficiently promoted the conductivity and stability and the electrochemical performance of prepared Bi₂O₃/C outperforms other reported Bi₂O₃ materials.

Metal (Li, Na, and K) ion batteries have significant applications in electronic storage devices. Among them, lithium-ion batteries

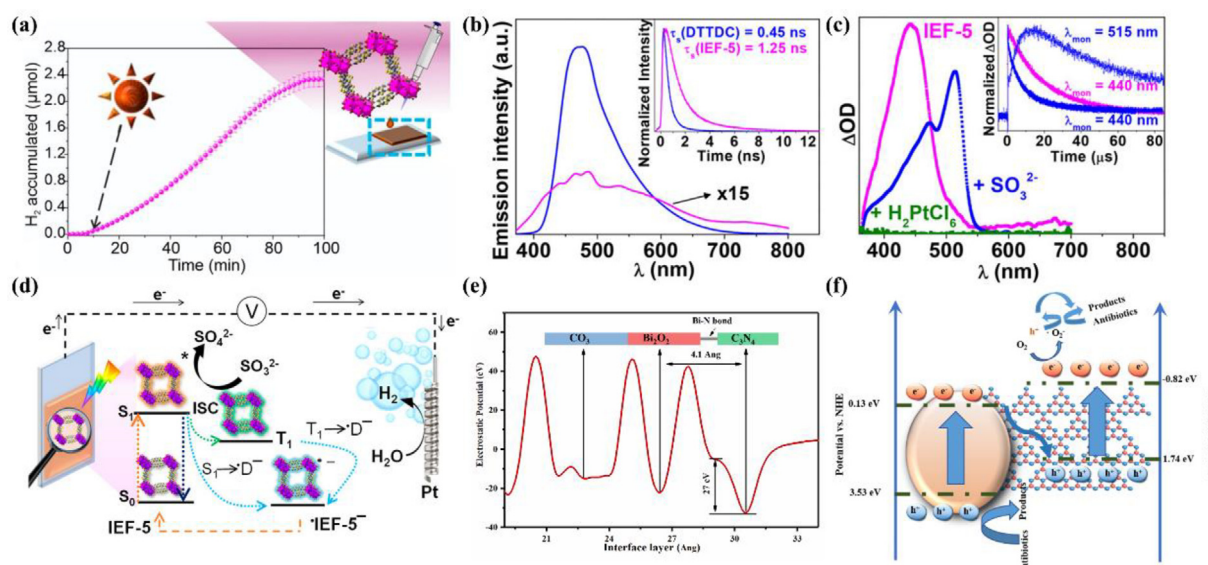


Fig. 6. (a) Photoelectrochemical H₂ production accumulated in 60 min under AM1.5 irradiation at 0.35 V. (b) Emission spectra ($\lambda_{\text{exc}} = 350$ nm) of DTTDC (blue) and IEF-5 (magenta) in solid. Inset: Decay traces ($\tau_{\text{exc}} = 372$ nm) of DTTDC and IEF-5. (c) TAS upon UV excitation ($\lambda_{\text{exc}} = 355$ nm) for IEF-5 (magenta) and using H₂PtCl₆ (green) as electron acceptor or Na₂SO₃ (blue) as electron donor. Inset: Triplet lifetimes monitored at 440 and 520 nm in the absence (magenta) or in the presence (blue) of NaSO₃. (d) Scheme of photo(electro)catalytic H₂ production mechanism, where S₀ is the fundamental state, S₁ the singlet excited state, T₁ the triplet excited state, D⁻ the radical anion, and ISC the intersystem crossing. (e) The electrostatic potentials of BO/CN with Bi-N bonds. (f) Possible mechanism for pollutant degradation and electron flow by BO/CN. Reprinted with permission from Ref. [28,39]. Copyright 2020, American Chemical Society and Elsevier.

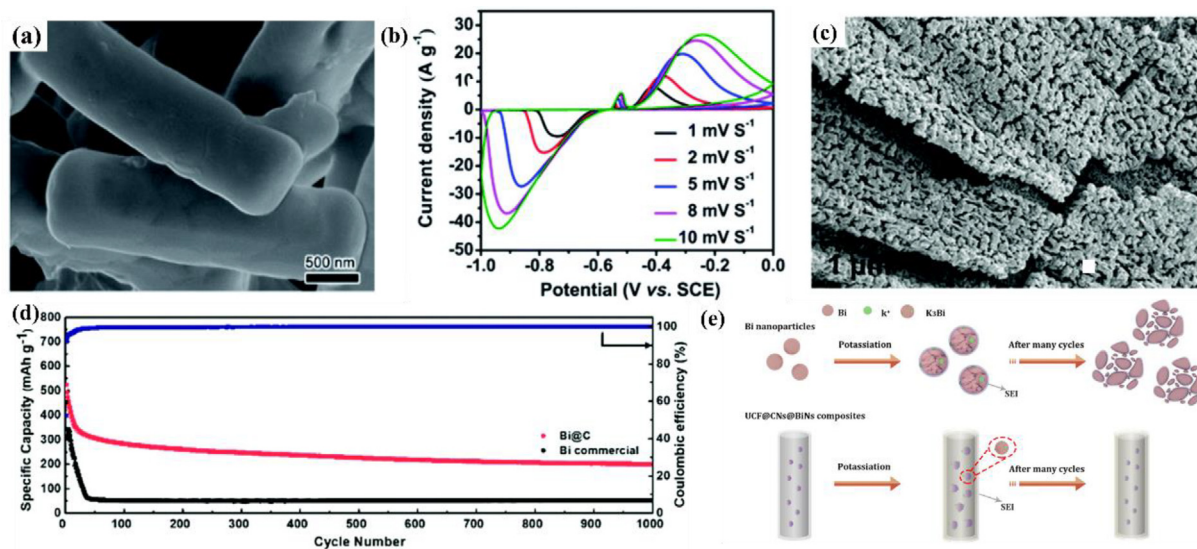


Fig. 7. Electrochemical energy storage of Bi-MOF-derivatives. (a and b) $\text{Bi}_2\text{O}_3/\text{C}$ derived from CAU-17 for supercapacitors: morphology illustrations and cyclic voltammograms at different scan rates. (c and d) Bi/C derived from Bi-BTC for lithium-ion batteries: morphology illustrations and cycling performance at a current density of 3000 mA g^{-1} . (e) Schematic illustration of traditional Bi and the UCF@CNs@BiN composite electrode during potassiation and depotassiation processes. Reprinted with permission from Ref. [41,71,73]. Copyright 2020, the Royal Society of Chemistry, and American Chemical Society.

(LIBs) have received widespread concerns due to the high voltage, excellent cycle life and low environmental pollution [111]. But traditional LIBs are hard to fill the bill of high-power density and energy density when they are applied in the modernize electrical energy storage (EES), such as electrical vehicles and stationary EES [112]. Recently, Bi-based electrodes have captured attractive attention due to their nearly $3800 \text{ mA h cm}^{-3}$ theoretical capacities. However, Bi-based electrodes usually suffer from the poor recyclability, thus leading to insufficient retention upon Li cycling. Benefiting from high porosity with carbonaceous components preventing the aggregation of nanoparticles during lithiation/delithiation, Bi-MOFs derivatives can achieve high capacity and simultaneously retain desired cycle life.

Yang et al. [75] studied the electrochemical performance of Bi-BTC derived $\text{Bi}_2\text{S}_3/\text{C}$ nanorods as anode material for LIBs. Owing to the integrated merits of Bi_2S_3 nanoparticles and carbon matrix, the $\text{Bi}_2\text{S}_3/\text{C}$ nanorods exhibited a reversible capacity of 1631 mA h g^{-1} at 100 mA g^{-1} and maintained 765 mA h g^{-1} up to 100 cycles. This performance was much higher than that of the pristine Bi_2S_3 . Furthermore, the carbon-coated bismuth nanospheres (Bi/C) have displayed high potential as a lithium battery anode [42]. The Bi-BTC derived Bi/C demonstrated stable capacity with 515 mA h g^{-1} after 150 cycles at 100 mA g^{-1} . Modulating the morphology could significantly affect the performance and stability. Kim et al. [41] reported Bi-BTC derived Bi/C nanoplates exhibited 200 mA h g^{-1} capacity after 1000 cycles at 3000 mA g^{-1} (Fig. 7c and d). The advantage of MOF-combustion is that carbon matrices efficiently anchor Bi granules, suppressing the possible aggregation and alleviating the volume expansion (Fig. 7e). Such advantage also allows the architectural design of the advanced electrode materials for potassium-ion batteries (PIBs). As a proof of concept, Su et al. [71] designed novel ultrathin carbon film@carbon nanorods@Bi nanoparticle starting from CAU-17. The carbon nanorods could accelerate the ion transport and the ultrathin carbon film limited major solid electrolyte interface film formation on the outer surface of the anode. As a result, the UCF@CNs@BiN displayed outstanding cycling and rate performance at 100 mA g^{-1} and 1000 mA g^{-1} , respectively (a capacity decay of 0.038% per cycle over 600 cycles and a capacity decay of 0.036% per cycle after 7000 cycles). Sodium-ion batteries (SIBs) are promising substitutes

for commercialized lithium-ion batteries due to abundant sodium reserves. Recently, Wen et.al. reported using Bi-BTC as precursors to synthesize $\text{Bi}_2\text{Te}_3@\text{C}$ composite [74]. The composite inherited the morphology of the Bi-BTC MOFs and all Bi_2Te_3 nanoparticles were uniformly distributed in the carbon support. When used as an anode for SIBs, the as-synthesized $\text{Bi}_2\text{Te}_3@\text{C}$ composite exhibited a reversible capacity of $236.4 \text{ mA h g}^{-1}$ at 100 mA g^{-1} after 100 cycles.

5.3. Biomedical imaging and drug delivery

CT imaging provides visualization of internal structures, including the liver, bone, lungs and so on. Commonly, CT contrast agents with the high atomic number elements, involving iodine, barium and bismuth, are kind of desired materials to attenuate X-rays and enhance the contrast. Bi-NU-901, with a similar topology structure to Zr-NU-901, has been selected as CT contrast agents [33]. CT phantom investigations displayed that Bi-NU-901 possessed higher X-ray attenuation factors compared with Zr-NU-901 and commercially iodixanol. A higher X-ray attenuation factors contributed to the less doses use of contrast agents. Bi-MOFs provide an interesting platform for designing contrast media in the future.

In addition, MOFs with high loading capacities and biocompatibility can provide an ideal platform for drug delivery. CAU-7 was developed to deliver anticancer drugs sodium dichloroacetate (DCA) and α -cyano-4-hydroxycinnamic acid (α -CHC) [32]. These drugs could be encapsulated in CAU-7 with modest efficiency (33 and 9 wt%, respectively) and slow rate of release (Fig. 8a-f). Studies suggested that CAU-7 capsules could improve the internalization of DCA and α -CHC, thereby enhancing its cytotoxicity for HeLa cells (Fig. 8g).

5.4. Fluorescence sensing

The use of MOFs as fluorescence sensing materials represents one of the hot applications in MOFs research. The structural and functional tunability of MOFs could correlate the emission intensities with the concentrations of the emission centers, making these frameworks suitable for practical applications. The emission

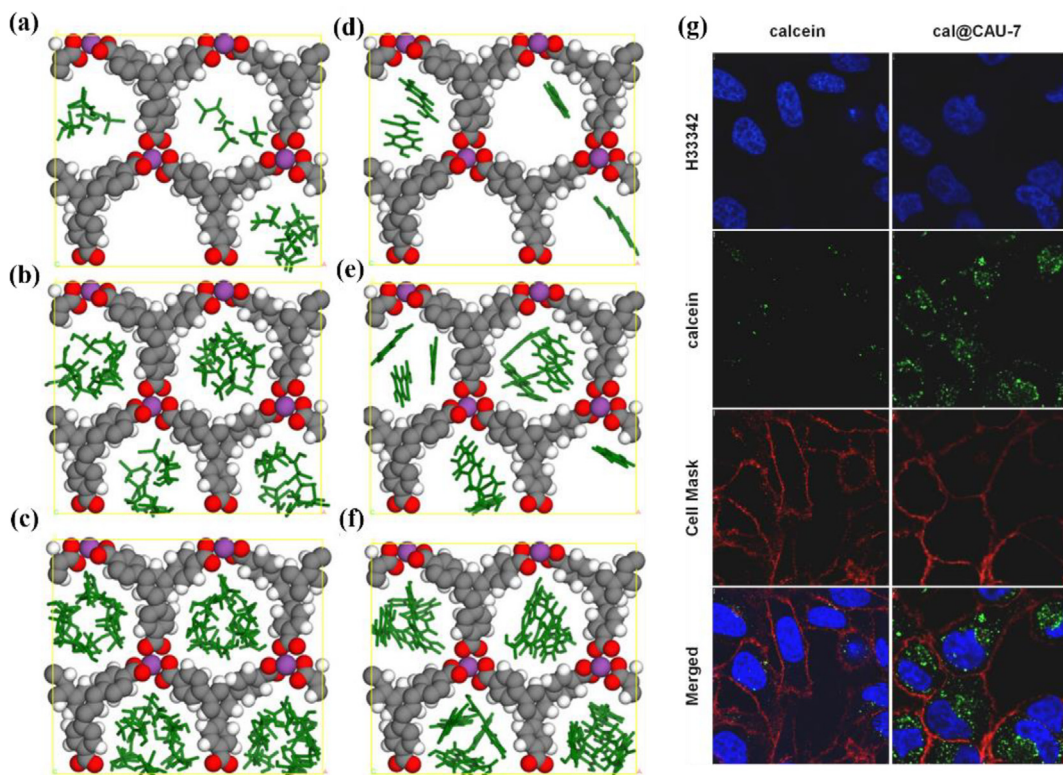


Fig. 8. Snapshots of DCA (a–c) and α -CHC (d–f) in CAU-7 at different loadings: (a) 121 mg g⁻¹ or 10.8 wt%, (b) 307 mg g⁻¹ or 23.5 wt%, (c) saturation with 500 mg g⁻¹ or 33.3 wt%, (d) 42 mg g⁻¹ or 4.0 wt%, (e) 126 mg g⁻¹ or 11.2 wt%, and (f) saturation with 248 mg g⁻¹ or 19.9 wt%. The drug molecules are represented in the green-stick mode. (g) Confocal microscopy images of HeLa cells incubated with cal@CAU-7 or free calcein for 24 h. Reprinted with permission from Ref. [32]. Copyright 2020, the Royal Society of Chemistry, and American Chemical Society.

centers can be trivalent rare-earth (RE^{3+}) ions or organic ligands. As for the Bi-based fluorescent MOFs, the fluorescence originates from both of organic ligands and the incorporated RE^{3+} ions in Bi³⁺ matrices.

As discussed above, Bi-MOFs present high biocompatibility towards biological imaging due to low toxicity and insolubility. H₄TBAPy is a typical pyrene fluorescent ligand with electron-rich property and larger conjugated pyrene nuclei. For example, Qing et al [30] prepared intrinsically fluorescent Bi-TATBy as a potential sensor for the selective recognition of biothiol molecules, including cysteine (Cys), glutathione (GSH), and homocysteine (Hcy) (Fig. 9a). And the detection limit was estimated to be 1.41, 1.71, and 1.10 μ M for Cys, GSH, and Hcy, respectively (Fig. 9b-d). The mutual effects between –SH group in biothiols and Bi-TATBy played an important role in the characteristic “turn on” fluorescence for biothiol molecules. Based on the CCK-8 assay and biological images, Bi-TATBy presented weak cytotoxicities and negligible impact on the surface marker detection, exhibiting promising potential in the biological field as a fluorescent probe.

Immobilizing or encapsulating the trivalent lanthanides as the signal reporters into the host framework is another strategy to design and synthesize fluorescent MOFs. Bi(III) cation possesses similar ionic radii and coordination behavior with the trivalent lanthanides. Bismuth-based organic compounds or coordination polymers have been successfully utilized as hosts for lanthanides ions. Earlier in 2012, Bi(III) based frameworks constructed by 2,6-pyridinedicarboxylic acid and 1,4-benzenedicarboxylic acid acted as hosts to encapsulate different metal ions (Eu³⁺ or Tb³⁺) [113]. Recently, E. Knope et al [31] explored the doping of lanthanide (Ln) ions into three bismuth(III)-thiophenedicarboxylates. Two of doped phases encapsulating the Ln metal center with formula Hpy[Bi_{1-x}Ln_x(TDC)₂(H₂O)]·1.5H₂O (Ln = Nd, Sm, Eu, Tb, Dy, and

Yb), and (Hpy)₂[Bi_{0.99}Eu_{0.01}(TDC)₂(HTDC)]·0.36H₂O were reported, displaying the typical visible and NIR luminescence. The europium doped phases’ lifetime was comparable to that of other europium only compounds. Despite these developments, it is still a significant challenge to achieve high charge mobility and electron conductivity and simultaneously obtain high quantum yields for the introduction of Ln emission centers into bismuth-based MOFs [114].

5.5. Adsorption and separation

The studies about the storage of fuel gases including methane and hydrogen persistently have captured worldwide researchers’ attentions [6,104,115]. Methane adsorption based on Bi-MOFs was firstly reported in 2014 [61]. As a high-density system, Bi-MOF NOTT-220 exhibited an uptake capacity of 189 V(STP)/V at 35 bar and 293 K. This phenomenon confirmed the potential of Bi-MOFs for application to methane adsorption, thus potentially implementing high volumetric gas uptake. In addition, the efficient separation of hydrogen from the synthetic gas, including CH₄, CO, CO₂ and H₂O is a huge challenge. Zhang et al. [116] demonstrated that CAU-17 displayed extremely high CH₄/H₂ selectivity based on grand canonical Monte Carlo simulations and dispersion-corrected DFT. This separation efficiency was superior to those of classic porous MOFs, such as IRMOF-1, Cu-BTC and ZIF-8. Such an advantage could be mainly ascribed to the rectangle channel predominantly of CAU-17 for CH₄ loading, which selectively adsorbed CH₄ over H₂.

Bi-MOFs also are promising for selectively capturing the toxic substances from water and gases. In 2018, a detailed study of SeO₃²⁻ anions adsorption showed that CAU-17 possessed ultrahigh adsorption capacity of 255.3 mg g⁻¹ and fast kinetics, which was much higher than previous studies [117]. Gas storage experiments

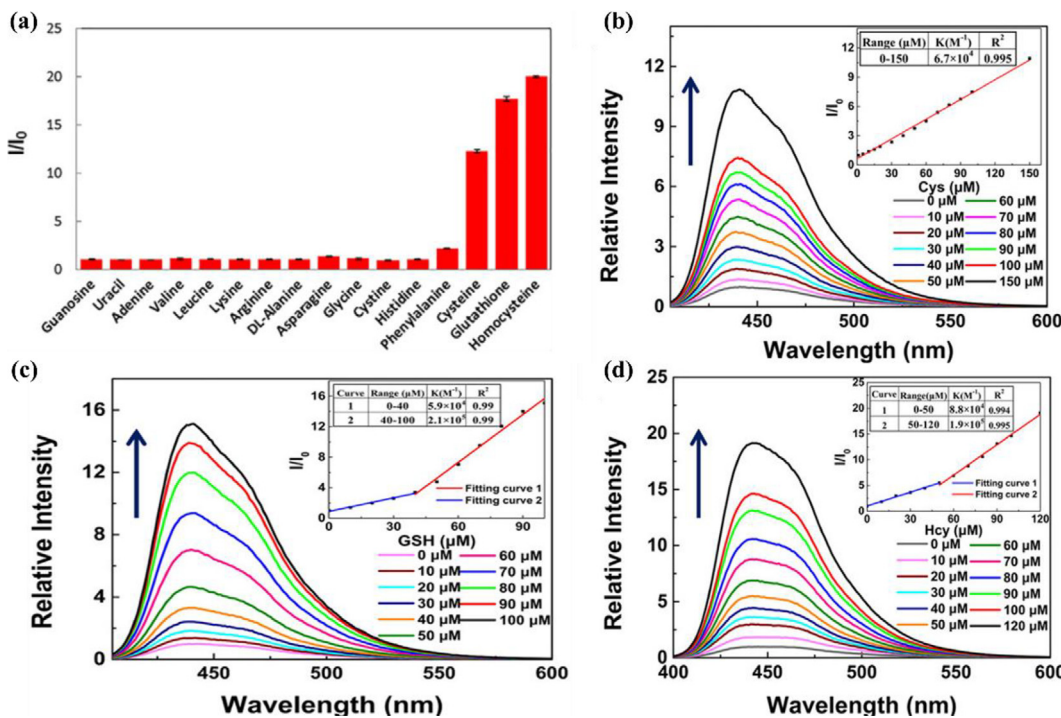


Fig. 9. (a) Selectivity of the Bi-TBAPy to different amino acids. The data represent the mean \pm SD of at least three independent experiments. (b) Families of fluorescence spectra of Bi-TBAPy dispersing in EtOH upon the addition of 150 μ M Cys recorded at room temperature ($\lambda_{\text{ex}} = 396$ nm). The inset shows linear fitting of the relative fluorescence intensity as the concentration of Cys in the range of 0–100 μ M; (c) families of fluorescence spectra of Bi-TBAPy dispersing in EtOH upon the addition of 100 μ M GSH recorded at room temperature ($\lambda_{\text{ex}} = 396$ nm). The inset shows linear fitting of the relative fluorescence intensity as the concentration of GSH in the range of 0–100 μ M; (d) families of fluorescence spectra of Bi-TBAPy dispersing in EtOH upon the addition of 120 μ M Hcy recorded at room temperature ($\lambda_{\text{ex}} = 396$ nm). The inset shows linear fitting of the relative fluorescence intensity as the concentration of Hcy in the range of 0–120 μ M. Reprinted with permission from Ref. [30]. Copyright 2019, American Chemical Society.

on Bi-MOFs have also been expended to the adsorption of acidic gases H_2S . As expected, the best excess H_2S uptake reported to date for a MOF was investigated in SU-101 with robust structure. The calculated total uptake values for H_2S was 15.95 mmol g⁻¹. However, due to the formation of polysulfides inside the pores of SU-101, the H_2S uptake was decreased to 0.2 mmol g⁻¹ in the second cycle reaction.

6. Insights and perspectives

6.1. Bi-MOFs

6.1.1. Synthesis

In all of reported instances, hydrothermal and solvothermal methods are generally used. Commonly, organic ligands and Bi(III) salt are mixed in suitable solvents and put into Teflon-lined steel autoclave or sealed Pyrex vial and heated to a designed temperature for several hours or days. More reaction conditions of hydrothermal and solvothermal methods are listed in Fig. 10. Solvent plays a vital role in the nucleation and crystallization of Bi-MOFs with permanently porous, embracing either methanol (CAU-7 [27], CAU-17 [48], SU-100 [60]), DMF with toluene (CAU-33 [118]), DMF with water (CAU-35 [59]), DMF with ethanol (Bi-NU901 [33]) and DMF with acetonitrile (NOTT-220 [61]). Amongst the solvents, methanol and DMF are promising candidates. A challenge in the preparation of Bi-MOFs is to enhance the solubility of bismuth salts and control the hydrolysis reactivity of Bi(III). According to the cases of zirconium-based MOFs, the introduction of modulators such as dilute nitric acid or monocarboxylic acids is an efficient approach to regulate the coordination equilibrium

[119]. The addition of dilute nitric acid aims to avoid the formation of bismuth hydroxides and maintains the necessary Bi(III) cation concentration for the construction of open-framework in the solution [55]. A representative instance of adopting this regulated synthesis strategy to fabricate Bi-MOF was reported by Yang et al. in 2014 (Fig. 10b) [61]. In this work, NOTT-220 was synthesized by using biphenyl-3,3',5,5'-tetracarboxylate as ligands with dilute nitric acid and piperazine as modulators. The piperazine is employed to compete with organic ligands for Bi(III) ions to hinder the coordination interaction, thus regulating the rate of nucleation and MOFs growth [120]. Through a high-throughput investigation, Norbert Stock et al. [118] used 1,2,4,5-tetrakis-(4-carboxyphenyl) benzene (H₄TCPB) organic linkers to synthesize CAU-33 with toluene as additives (Fig. 10e). By this synthesis control, a new structure [Bi₄(O)₂(OH)₂(H₂TCPB)(TCPB)(H₂O)₂]·xH₂O with rod morphology was obtained and it was found that the additions of a small amount of toluene could improve the product yield efficiently.

In terms of large-scale synthesis for industrial application, some novel methods should be adopted for the fabrication of crystalline bismuth-based MOFs, such as microwave technology [27,48], ionothermal method [121], mechanochemistry [122], water-based room temperature synthesis [123], etc. These strategies address fundamental synthesis procedures, covering safer solvents and reagents, higher energy efficiency and more environmentally process. In fact, large-scale synthesis of SU-101 in a water solution under ambient conditions (room temperature and atmospheric pressure) has been achieved (Fig. 10h) [69]. The estimated space-time-yield under such conditions is up to 5 kg m⁻³ day⁻¹. Complementary to this aspect, the readers are also suggested to read other reviews about the construction of MOFs [124,125].

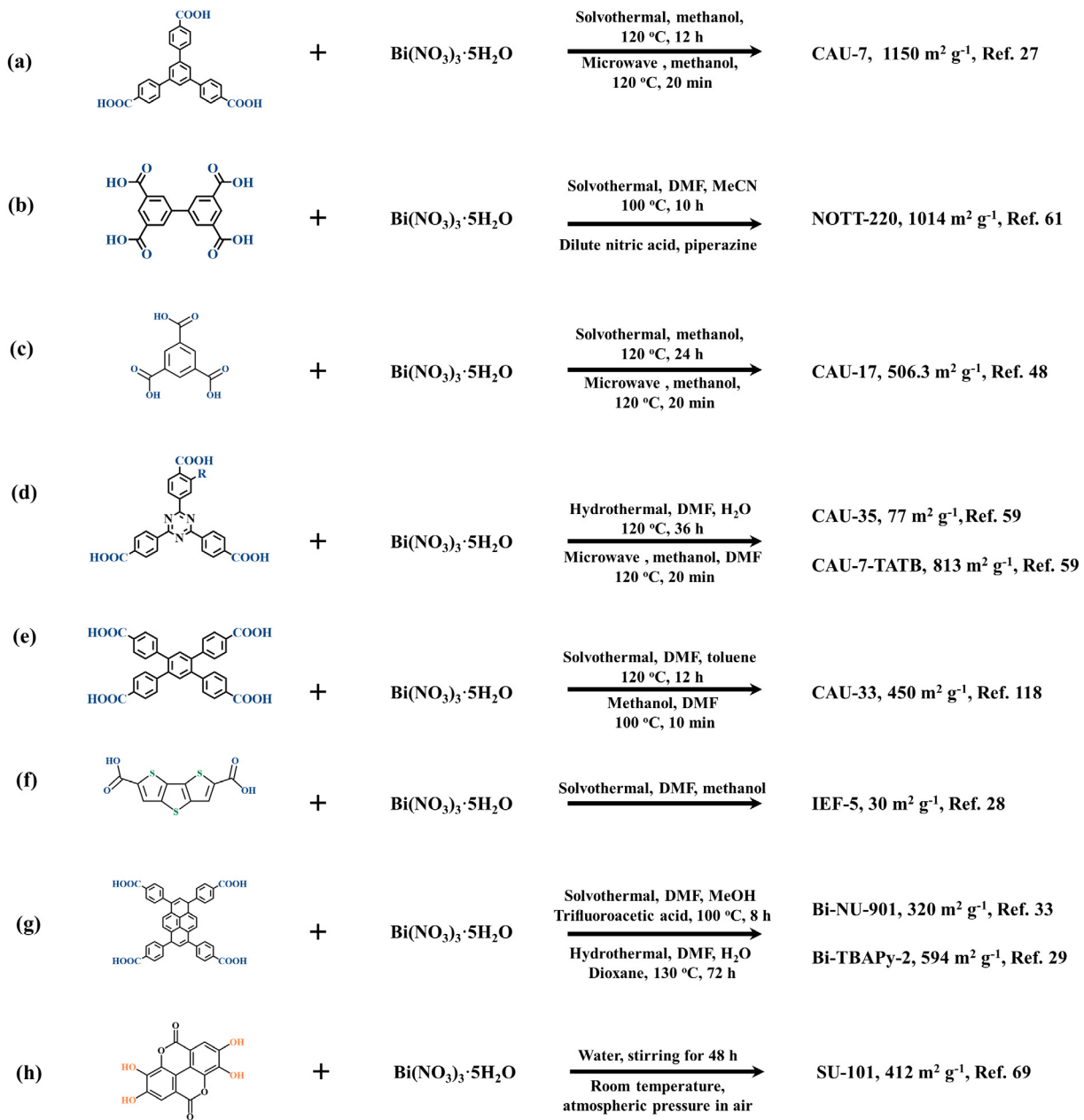


Fig. 10. Some important synthetic process of Bi-MOFs.

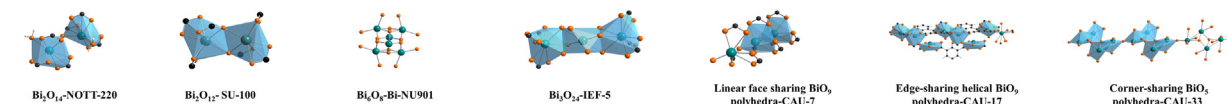
Besides, the structural characterization of Bi-MOFs is also of great challenge. The use of Bi(III) cation often results in the production of micro- or nanocrystalline coordination polymers, whose structures are seldom possible for the direct structure analysis by single-crystal X-ray diffraction. In some cases, including CAU-7 [27], CAU-33 [118], and SU-100 [60], ADT [126] based on transmission electron microscope (TEM) provides a conducive method in acquisition of detailed structure from discrete micro- or nanosized crystals. Some nonstandard approaches such as synchrotron microdiffraction [127], ligand-replacement strategy [59,60,128] and computational assisted structure determination [129] are also needed to be developed allowing a structure determination of micro- or nanosized crystals.

6.1.2. Structure

In 1984, bismuth oxalate crystals were fabricated by Polla et al. [57] via a simple conventional solution reaction. Subsequently, a

series of Bi(III) compounds have been performed but bismuth-based MOFs are rather limited [49,52,57,130–133]. Although the first Bi-MOF with the molecular formula $\text{Bi}(\text{C}_2\text{O}_4)\text{OH}$ was reported in 2008 [130], the reported intrinsic Bi-MOFs with permanent porosity are less than 10 (CAU-7, NOTT-220, CAU-17, CAU-33, Bi-NU-901, SU-100, Bi-TBAPy-2 and SU-101). Notably, most of reported Bi-MOFs are relied on Bi-oxygen coordination bonds, while the nitrogen or phosphonate ligands are scarcely explored. Carboxylates are widely utilized in the fabrication of Bi-MOFs but phosphonate ligands exhibit strong chelate ability [134]. This outstanding feature could be applied in connection with Bi(III) cation to construct MOFs with regular structures and excellent chemical durability [135]. With regard to framework structure, five types of finite Bi-clusters (i.e. Bi_6O_8 [33], Bi_8O_6 [30], $\text{Bi}_{12}\text{O}_{12}$ [60], $\text{Bi}_{20}\text{O}_{14}$ [61], Bi_3O_{24} [28]) and four infinite bismuth-oxo rods (i.e. linear face sharing BiO_9 polyhedra [27], edge-sharing helical BiO_9 polyhedra [48], a highly condensed linear chain of BiO_7 polyhedra [59],

Finite clusters and infinite polyhedra



Topology and frameworks

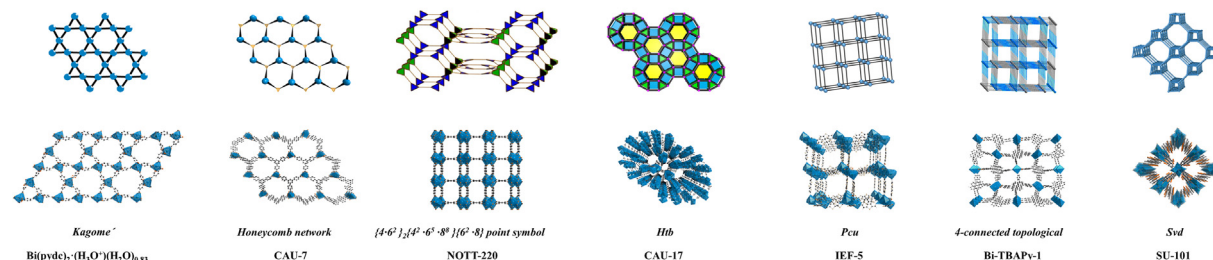


Fig. 11. Some representative clusters and polyhedra, topological networks, frameworks of Bi-MOFs.

corner-sharing BiO_5 polyhedra [118]) as unique inorganic building units have appeared in recent decade (Fig. 11). Furthermore, the structures of reported Bi-MOFs still show intriguing and variable structure with unpredictable topologies (Fig. 11).

Inspiring from advances in the chemistry of other MOFs, isoreticular principle and postsynthetic modification strategies (PSM) have been implemented to prepare bismuth-based MOFs with remarkable functionality. For the former, the replacement of metal ions in the SBUs is useful to construct isostructural MOFs. Indeed, after the appearance of NU-901-Zr, an isostructural NU-901-Bi was prepared based on $[\text{Bi}_6\text{O}_4(\text{OH})_4(\text{NO}_3)_6(\text{H}_2\text{O})](\text{H}_2\text{O})$ nodes and 1,3,6,8-tetrakis(p-benzoate)-pyrene (TBAPy) linkers [33]. Moreover, the utilization of prolonged ligands has also been regarded as a modulate strategies to construct MOFs with identical structures and functions. This approach was adopted by prolonging the original phenylene unit of CAU-17 to 2 phenylene unit (H_3BTC to H_3BPT) [60]. The obtained structure (termed SU-100) demonstrated a solvent dependent flexibility. For the latter, PSM has become sufficiently mainstream in the MOF field and a number of splendid researches have been performed to meet the requirements for specific applications [136,137]. However, the PSM in bismuth chemistry is still at an early stage. Only one example existed that eight different reagents were employed to modify CAU-7-TATB- NH_2 [59]. These reagents included several anhydrides, ethyl isocyanate, methanesulfonyl chloride, acetyl chloride, and two different sultones. As a result, five products of the PSM reactions were obtained. All the products remained crystalline structure but only CAU-7-TATB- NH_2 -AA and CAU-7-TATB- NH_2 -VA remained porous, which could be ascribed to the acidic groups occupying the pores of CAU-7-TATB- NH_2 . To ensure the continuously emergence of Bi-MOFs with diverse frameworks and other SBUs, more methods such as topologies guided synthesis, isoreticular expansion, multiple organic functionalities and metal centers should be advanced.

6.1.3. Applications

To date, a series of MOFs have been explored as catalysts, nanocarriers for biomedical imaging and drug delivery, sensors, adsorbents and energy storage materials. Combining the intrinsic advantages of bismuth element, the capabilities of Bi-MOFs have been comprehensively studied.

Firstly, the closed shell character of $\text{Bi}(\text{III})$ cation may result in a LLCT mechanism in photocatalysis and photoelectrocatalysis. This is distinguished from the widely proved LCMT mechanism of MOFs, such as MIL-125 (Ti), UiO-66, ZIF-67 etc. Therefore, more attentions may be focused on the selection of linkers with extensive light absorption and electron rich rigid core. Moreover, Bi-MOFs are promising electrocatalysts for ECCR but the poor stability and low conductivity limit their further application.

Then, compared to a variety of MOFs which have been utilized as nanocarriers for biomedical imaging and drug delivery, Bi-MOFs possess some nature advantages [138–140]. First, most of bismuth coordination polymers are biologically safe and nontoxic due to lower toxicity compared with sodium chloride [141]. Second, bismuth compounds are intrinsically insoluble in neutral aqueous solution and exhibit the inhibition of pathogenic bacteria, making it possible to simultaneously meet high biocompatibility and low accumulation in cells [46]. Therefore, Bi-MOFs have been a potential candidate used in medicine and biological field. Although a series of bismuth compounds have been approved for drug usage, only a few of studies have used Bi-MOFs for drug delivery and biosensing.

Moreover, Bi-MOFs have been promising for in proton-conducting [142] nonlinear optical materials [143], fluorescent sensors and selective adsorption for toxic ions and gases [117,144]. Compared with other MOFs subclasses, including ZIFs, Fe-MOFs, Cu-MOFs, Zr-MOFs and Ti-MOFs, Bi-MOFs are rarely explored. With these unique properties, more exhaustive investigations are expected to explore the full potential.

6.2. Derivatives

Bi-MOFs have been demonstrated as an ideal platform to fabricate bismuth-based nanostructures. As highlighted in this review, thermal transformation and *in situ* electrochemical transformation have been described to be two effective ways to derive bismuth-based porous nanostructures with uncomplicated synthetic processes. To date, the studies of Bi-MOFs derivatives mainly concentrate on bismuth nanoparticles and oxides with nanorod morphology. While some studies on Bi-MOFs derived carbonate-hydroxides, sulfides and oxyhalides are available, most of studies are often limited to tritopic-carboxylate based MOFs such as CAU-17 or CAU-7. Therefore, the exploration of alternative

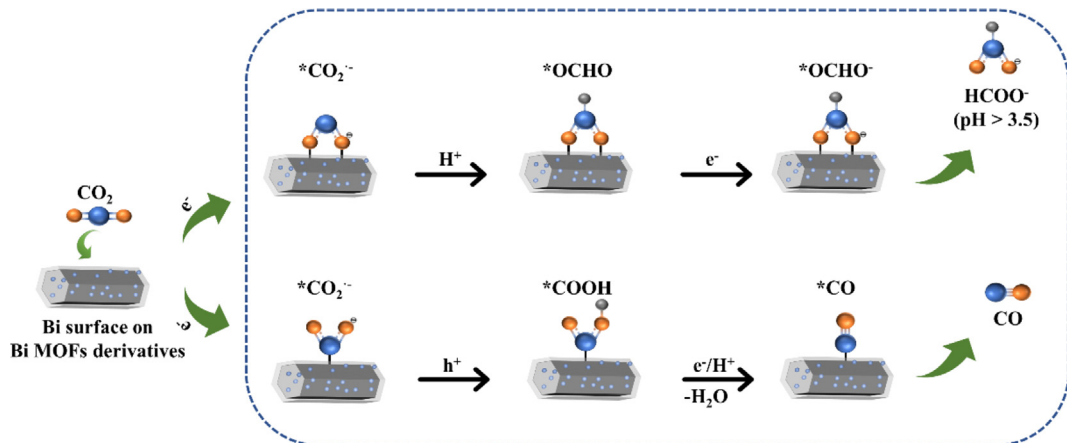


Fig. 12. Possible reaction pathways for electrochemical CO_2 reduction reaction to formate and CO .

Bi-MOFs for the derivation of various nanostructures/nanocomposites is desirable. Furthermore, there is a lack of precise control over the composition and morphology due to the complexed conversion procedure from Bi-MOFs to derivatives. Theoretical prediction combined with *in situ* characterization (e.g., *in situ* TEM and *in situ* Raman spectroscopy) might in-depth understand the transformation process and significantly accelerate the development of this filed.

Bi-MOFs derivatives ordinarily inherit the advantages of parent MOFs such as high surface area, unique morphology and tailored components, thus giving rise to their functional performance in energy-related applications. For example, in energy storage devices, the Bi-MOFs derived metal (or metal compounds)/carbon hybrids can alleviate the low conductivity and high-volume expansion, thereby achieving high capacity and cyclic stability. As for the ECRR, bismuth-based derivatives exhibit outstanding activity and selectivity for electrochemical CO_2 reduction to C1 products. In this process, if they are thermodynamically in favor of the adsorption of $^*\text{COOH}$ over $^*\text{OCHO}$, CO is the main product. Otherwise, the formate becomes the predominant reduction product (Fig. 12). Up to now, Bi-MOFs derivatives have the maximum selectivity of $\approx 97\%$ for CO and $\approx 100\%$ for formate [34,38,92]. Rationally increasing active site density and activity via suitable compositional and conversion design, and the optimization of ECRR performance at the cell level (i.e., flow cells or MEA cells) are recommended in further work. Finally, MOFs derived nanomaterials recently have captured emerging attentions in environment field, such as wastewater treatment [39], air purification [145] and target-specific sensing [146]. With continuous progress on Bi-MOFs derivatives, the widely use of Bi-MOFs derivatives for environment application is highly feasible to be expected.

7. Conclusion

Based on a range of selected examples, the recent progress (2012–2020) in the chemistry and engineering of Bi-MOFs and their derivatives has been proposed. As we described in the previous part, Bi-MOFs and their derivatives have presented preeminent chemical and physical properties due to intrinsic merits of Bi metal, such as non-toxicity, biocompatibility, high volume capacity, and environmental friendliness. From the point of engineering, they displayed superior performance in the catalysis, energy storage, biomedical imaging, drug delivery, fluorescence sensing, adsorption and separation field. By comprehensively analyzing these studies, important perspectives are proposed and directions for further investigations are suggested. Overall, this critical review

provides enlightenment to researchers in offering numerous possibilities for the evolution of novel ideas and applications in the field of MOFs.

Declaration of Competing Interest

The authors declare that they have no known competing financial interests or personal relationships that could have appeared to influence the work reported in this paper.

Acknowledgments

This work was supported by the National Natural Science Foundation of China (No. 51521006, 51709101, 51508177, 51579098, 51779090), the National Program for Support of Top-Notch Young Professionals of China (2014), Hunan Provincial Science and Technology Plan Project (No. 2016RS3026, 2017SK2243), the Program for Changjiang Scholars and Innovative Research Team in University (IRT-13R17) and the Three Gorges Follow-up Research Project (2017HXXY-05).

References

- [1] O.M. Yaghi, H. Li, *J. Am. Chem. Soc.* 117 (1995) 10401–10402.
- [2] S.-I. Noro, S. Kitagawa, M. Kondo, K. Seki, *Angew. Chem. Int. Ed.* 39 (2000) 2081–2084.
- [3] O.M. Yaghi, M. O'Keeffe, N.W. Ockwig, H.K. Chae, M. Eddaoudi, J. Kim, *Nature* 423 (2003) 705–714.
- [4] S. Yuan, L. Feng, K. Wang, J. Pang, M. Bosch, C. Lollar, Y. Sun, J. Qin, X. Yang, P. Zhang, Q. Wang, L. Zou, Y. Zhang, L. Zhang, Y. Fang, J. Li, H.C. Zhou, *Adv. Mater.* 30 (2018) e1704303.
- [5] D. Jiang, *Chem.* 6 (2020) 2461–2483.
- [6] H. Furukawa, K.E. Cordova, M. O'Keeffe, O.M. Yaghi, *Science* 341 (2013) 1230444.
- [7] M.Y. Masoomi, A. Morsali, A. Dhakshinamoorthy, H. Garcia, *Angew. Chem. Int. Ed.* 58 (2019) 15188–15205.
- [8] W. Wang, Q. Niu, G. Zeng, C. Zhang, D. Huang, B. Shao, C. Zhou, Y. Yang, Y. Liu, H. Guo, W. Xiong, L. Lei, S. Liu, H. Yi, S. Chen, X. Tang, *Appl. Catal. B* 273 (2020).
- [9] M. Duan, L. Jiang, G. Zeng, D.B. Wang, L. Tang, *Appl. Mater. Today* 19 (2020) 100564.
- [10] M.J. Kalmutzki, C.S. Diercks, O.M. Yaghi, *Adv. Mater.* 30 (2018) 1704304.
- [11] A. Dhakshinamoorthy, Z. Li, H. Garcia, *Chem. Soc. Rev.* 47 (2018) 8134–8172.
- [12] J.D. Xiao, H.L. Jiang, *Acc. Chem. Res.* 52 (2019) 356–366.
- [13] S. Ye, M. Yan, X. Tan, J. Liang, G. Zeng, H. Wu, B. Song, C. Zhou, Y. Yang, H. Wang, *Appl. Catal. B* 250 (2019) 78–88.
- [14] H. Wang, Z. Zeng, P. Xu, L. Li, G. Zeng, R. Xiao, Z. Tang, D. Huang, L. Tang, C. Lai, D. Jiang, Y. Liu, H. Yi, L. Qin, S. Ye, X. Ren, W. Tang, *Chem. Soc. Rev.* 48 (2019) 488–516.
- [15] K. Lu, T. Aung, N. Guo, R. Weichselbaum, W. Lin, *Adv. Mater.* 30 (2018) 1707634.
- [16] L.J. Murray, M. Dinca, J.R. Long, *Chem. Soc. Rev.* 38 (2009) 1294–1314.
- [17] H. Yi, M. Yan, D.L. Huang, G.M. Zeng, C. Lai, M.F. Li, X.Q. Huo, L. Qin, S.Y. Liu, X. G. Liu, B.S. Li, H. Wang, M.C. Shen, Y.K. Fu, X.Y. Guo, *Appl. Catal. B* 250 (2019) 52–62.

- [18] S. Liu, X.F. Lu, J. Xiao, X. Wang, X.W.D. Lou, *Angew. Chem. Int. Ed.* **58** (2019) 13828–13833.
- [19] H.B. Wu, X.W. Lou, *Sci. Adv.* **3** (2017).
- [20] S. Dang, Q.-L. Zhu, Q. Xu, *Nat. Rev. Mater.* **3** (2017).
- [21] H. Wang, H. Wang, Z. Wang, L. Tang, G. Zeng, P. Xu, M. Chen, T. Xiong, C. Zhou, X. Li, D. Huang, Y. Zhu, Z. Wang, J. Tang, *Chem. Soc. Rev.* **49** (2020) 4135–4165.
- [22] P. Xu, G.M. Zeng, D.L. Huang, C.L. Feng, S. Hu, M.H. Zhao, C. Lai, Z. Wei, C. Huang, G.X. Xie, Z.F. Liu, *Sci. Total Environ.* **424** (2012) 1–10.
- [23] P. Xu, M. Chen, C. Lai, G. Zeng, D. Huang, H. Wang, X. Gong, L. Qin, Y. Liu, D. Mo, E. *Science Nano* (2019).
- [24] N. Han, P. Ding, L. He, Y. Li, Y. Li, *Adv. Energy Mater.* **10** (2019).
- [25] Z. Song, L. Zhang, K. Doyle-Davis, X. Fu, J.L. Luo, X. Sun, *Adv. Energy Mater.* (2020).
- [26] G.G. Briand, N. Burford, *Chem. Rev.* **99** (1999) 2601–2658.
- [27] M. Feyand, E. Mugnaioli, F. Vermoortele, B. Bueken, J.M. Dieterich, T. Reimer, U. Kolb, D. de Vos, N. Stock, *Angew. Chem. Int. Ed.* **51** (2012) 10373–10376.
- [28] A. García-Sánchez, M. Gomez-Mendoza, M. Barawi, I.J. Villar-Garcia, M. Liras, F. Gándara, V.A. de la Peña O’Shea, *J. Am. Chem. Soc.* **142** (2019) 318–326.
- [29] Y. Xiao, X. Guo, J. Liu, L. Liu, F. Zhang, C. Li, Chin. *J. Catal.* **40** (2019) 1339–1344.
- [30] Q.L. Guan, Y.H. Xing, J. Liu, C. Han, C.Y. Hou, F.Y. Bai, *J. Phys. Chem. C* **123** (2019) 23287–23296.
- [31] A.K. Adcock, B. Gibbons, J.D. Einkauf, J.A. Bertke, J.F. Rubinson, D.T. de Lill, K.E. Knopke, *Dalton Trans.* **47** (2018) 13419–13433.
- [32] C. Orellana-Tavra, M. Koppen, A. Li, N. Stock, D. Fairén-Jimenez, *ACS Appl. Mater. Interfaces* **12** (2020) 5633–5641.
- [33] L. Robison, L. Zhang, R.J. Drout, P. Li, C.R. Haney, A. Brikha, H. Noh, B.L. Mehdi, N.D. Browning, V.P. Dravid, Q. Cui, T. Islamoglu, O.K. Farha, *ACS Appl. Bio Mater.* **2** (2019) 1197–1203.
- [34] E. Zhang, T. Wang, K. Yu, J. Liu, W. Chen, A. Li, H. Rong, R. Lin, S. Ji, X. Zheng, Y. Wang, L. Zheng, C. Chen, D. Wang, J. Zhang, Y. Li, *J. Am. Chem. Soc.* **141** (2019) 16569–16573.
- [35] P. Deng, F. Yang, Z. Wang, S. Chen, Y. Zhou, S. Zaman, B.Y. Xia, *Angew. Chem. Int. Ed.* **59** (2020) 10807–10813.
- [36] J. Yang, X. Wang, Y. Qu, X. Wang, H. Huo, Q. Fan, J. Wang, L.-M. Yang, Y. Wu, *Adv. Energy Mater.* **10** (2020) 2001709.
- [37] D. Yao, C. Tang, L. Li, B. Xia, S.H. Qiao, *Adv. Energy Mater.* (2020).
- [38] C. Cao, D.-D. Ma, J.-F. Gu, X. Xie, G. Zeng, X. Li, S.-G. Han, Q.-L. Zhu, X.-T. Wu, Q. Xu, *Angew. Chem. Int. Ed.* **59** (2020) 15014–15020.
- [39] Z. Wang, H. Wang, Z. Zeng, G. Zeng, P. Xu, R. Xiao, D. Huang, X. Chen, L. He, C. Zhou, Y. Yang, Z. Wang, W. Wang, W. Xiong, *Appl. Catal. B* **267** (2020).
- [40] Z. Li, G. Huang, K. Liu, X. Tang, G. Zhang, J. Cleaner Prod. **272** (2020) 122892.
- [41] M.K. Kim, M.S. Kim, J.H. Park, J. Kim, C.Y. Ahn, A. Jin, J. Mun, Y.E. Sung, *Nanoscale* **12** (2020) 15214–15221.
- [42] W. Chai, W. Yin, K. Wang, W. Ye, B. Tang, Y. Rui, *Electrochim. Acta* **325** (2019).
- [43] C. Yuan, *Angew. Chem., Int. Ed.* (2020).
- [44] Q. Wang, D. Astruc, *Chem. Rev.* **120** (2020) 1438–1511.
- [45] L.M. Aguirre-Díaz, D. Reinares-Fisac, M. Iglesias, E. Gutiérrez-Puebla, F. Gándara, N. Snejko, M.Á. Monge, *Coord. Chem. Rev.* **335** (2017) 1–27.
- [46] Y. Yang, R. Ouyang, L. Xu, N. Guo, W. Li, K. Feng, L. Ouyang, Z. Yang, S. Zhou, Y. Miao, *J. Coord. Chem.* **68** (2015) 379–397.
- [47] M. Albat, N. Stock, *Inorg. Chem.* **57** (2018) 10352–10363.
- [48] A.K. Inge, M. Koppen, J. Su, M. Feyand, H. Xu, X. Zou, M. O’Keeffe, N. Stock, *J. Am. Chem. Soc.* **138** (2016) 1970–1976.
- [49] V. Stavila, R.L. Davidovich, A. Gulea, K.H. Whitmire, *Coord. Chem. Rev.* **250** (2006) 2782–2810.
- [50] M. Sadakiyo, T. Yamada, K. Honda, H. Matsui, H. Kitagawa, *J. Am. Chem. Soc.* **136** (2014) 7701–7707.
- [51] D.W. Lim, M. Sadakiyo, H. Kitagawa, *Chem. Sci.* **10** (2019) 16–33.
- [52] N. Yang, H. Sun, *Coord. Chem. Rev.* **251** (2007) 2354–2366.
- [53] J. Zhu, P.-Z. Li, W. Guo, Y. Zhao, R. Zou, *Coord. Chem. Rev.* **359** (2018) 80–101.
- [54] J.P. Zhang, Y.B. Zhang, J.B. Lin, X.M. Chen, *Chem. Rev.* **112** (2012) 1001–1033.
- [55] T. Devic, C. Serre, *Chem. Soc. Rev.* **43** (2014) 6097–6115.
- [56] A.C. Wibowo, M.D. Smith, H.C. zur Loyer, *Chem. Commun. (Camb.)* **47** (2011) 7371–7373.
- [57] D.T. Tran, D. Chu, A.G. Oliver, S.R.J. Oliver, *Inorg. Chem. Commun.* **12** (2009) 1081–1084.
- [58] A.C. Wibowo, S.A. Vaughn, M.D. Smith, H.C. zur Loyer, *Inorg. Chem.* **49** (2010) 11001–11008.
- [59] M. Köppen, O. Beyer, S. Wuttke, U. Lüning, N. Stock, *Dalton Trans.* **46** (2017) 8658–8663.
- [60] E.S. Grape, H. Xu, O. Cheung, M. Calmels, J. Zhao, C. Dejoie, D.M. Proserpio, X. Zou, A.K. Inge, *Cryst. Growth Des.* **20** (2019) 320–329.
- [61] M. Savage, S. Yang, M. Suyatin, E. Bichoutskaia, W. Lewis, A.J. Blake, S.A. Barnett, M. Schroder, *Chem. Eur. J.* **20** (2014) 8024–8029.
- [62] C.-W. Kung, T.C. Wang, J.E. Mondloch, D. Fairén-Jimenez, D.M. Gardner, W. Bury, J.M. Klingsporn, J.C. Barnes, R. Van Duyn, J.F. Stoddart, M.R. Wasielewski, O.K. Farha, J.T. Hupp, *Chem. Mater.* **25** (2013) 5012–5017.
- [63] M.H. Teplensky, M. Fantham, P. Li, T.C. Wang, J.P. Mehta, L.J. Young, P.Z. Moghadam, J.T. Hupp, O.K. Farha, C.F. Kaminski, D. Fairén-Jimenez, *J. Am. Chem. Soc.* **139** (2017) 7522–7532.
- [64] K.C. Stylianou, J. Rabone, S.Y. Chong, R. Heck, J. Armstrong, P.V. Wiper, K.E. Jelfs, S. Zlatogorsky, J. Bacsa, A.G. McLennan, C.P. Ireland, Y.Z. Khimyak, K.M. Thomas, D. Bradshaw, M.J. Rosseinsky, *J. Am. Chem. Soc.* **134** (2012) 20466–20478.
- [65] K.C. Stylianou, R. Heck, S.Y. Chong, J. Bacsa, J.T.A. Jones, Y.Z. Khimyak, D. Bradshaw, M.J. Rosseinsky, *J. Am. Chem. Soc.* **132** (2010) 4119–4130.
- [66] J. Ai, F.Y. Chen, C.Y. Gao, H.R. Tian, Q.J. Pan, Z.M. Sun, *Inorg. Chem.* **57** (2018) 4419–4426.
- [67] G. Mouchaham, L. Cooper, N. Guillou, C. Martineau, E. Elkaim, S. Bourrelly, P.L. Llewellyn, C. Allain, G. Clavier, C. Serre, T. Devic, *Angew. Chem. Int. Ed.* **54** (2015) 13297–13301.
- [68] E. Chen, M. Qiu, Y. Zhang, Y. Zhu, L. Liu, Y. Sun, X. Bu, J. Zhang, Q. Lin, *Adv. Mater.* **30** (2018) 1704388.
- [69] E.S. Grape, J.G. Flores, T. Hidalgo, E. Martinez-Ahumada, A. Gutierrez-Alejandre, A. Hautier, D.R. Williams, M. O’Keeffe, L. Ohrstrom, T. Willhammar, P. Horcajada, I.A. Ibarra, A.K. Inge, *J. Am. Chem. Soc.* **142** (2020) 16795–16804.
- [70] H. Yang, S. Ye, Z. Zeng, G. Zeng, X. Tan, R. Xiao, J. Wang, B. Song, L. Du, M. Qin, Y. Yang, F. Xu, *Chem. Eng. J.* **397** (2020).
- [71] S. Su, Q. Liu, J. Wang, L. Fan, R. Ma, S. Chen, X. Han, B. Lu, *ACS Appl. Mater. Interfaces* **11** (2019) 22474–22480.
- [72] W. Zhan, L. Sun, X. Han, *Nanomicro Lett.* **11** (2019) 1.
- [73] X. Yu, J. Sun, W. Zhao, S. Zhao, H. Chen, K. Tao, Y. Hu, L. Han, *RSC Adv.* **10** (2020) 14107–14112.
- [74] S. Wen, J. Zhao, Y. Zhu, J. Mao, H. Wang, J. Xu, *J. Alloys Compd.* **837** (2020).
- [75] W. Chai, F. Yang, W. Yin, S. You, K. Wang, W. Ye, Y. Rui, B. Tang, *Dalton Trans.* **48** (2019) 1906–1914.
- [76] X. Yu, J. Zhou, Q. Li, W.N. Zhao, S. Zhao, H. Chen, K. Tao, L. Han, *Dalton Trans.* **48** (2019) 9057–9061.
- [77] G. Huang, Z. Li, K. Liu, X. Tang, J. Huang, G. Zhang, *Catal. Sci. Technol.* **10** (2020) 4645–4654.
- [78] W.-W. Yuan, J.-X. Wu, X.-D. Zhang, S.-Z. Hou, M. Xu, Z.-Y. Gu, *J. Mater. Chem. A* **8** (2020) 24486–24492.
- [79] D. Farrusseng, S. Aguado, C. Pinel, *Angew. Chem. Int. Ed.* **48** (2009) 7502–7513.
- [80] J. Lee, O.K. Farha, J. Roberts, K.A. Scheidt, S.T. Nguyen, J.T. Hupp, *Chem. Soc. Rev.* **38** (2009) 1450–1459.
- [81] L. Jiao, Y. Wang, H.L. Jiang, Q. Xu, *Adv. Mater.* **30** (2018) e1703663.
- [82] M. Cheng, C. Lai, Y. Liu, G. Zeng, D. Huang, C. Zhang, L. Qin, L. Hu, C. Zhou, W. Xiong, *Coord. Chem. Rev.* **368** (2018) 80–92.
- [83] Y. Liu, Z. Liu, D. Huang, M. Cheng, G. Zeng, C. Lai, C. Zhang, C. Zhou, W. Wang, D. Jiang, H. Wang, B. Shao, *Coord. Chem. Rev.* **388** (2019) 63–78.
- [84] M. Köppen, A. Dhakshinamoorthy, A.K. Inge, O. Cheung, J. Ångström, P. Mayer, N. Stock, Eur. *J. Inorg. Chem.* **2018** (2018) 3496–3503.
- [85] H. Zhang, J. Li, Q. Tan, L. Lu, Z. Wang, G. Wu, *Chem. Eur. J.* **24** (2018) 18137–18157.
- [86] X. Xiao, L. Zou, H. Pang, Q. Xu, *Chem. Soc. Rev.* **49** (2020) 301–331.
- [87] S. Ye, G. Zeng, X. Tan, H. Wu, J. Liang, B. Song, N. Tang, P. Zhang, Y. Yang, Q. Chen, X. Li, *Appl. Catal. B* **269** (2020).
- [88] X.R. Zhou, Z.T. Zeng, G.M. Zeng, C. Lai, R. Xiao, S.Y. Liu, D.L. Huang, L. Qin, X.G. Liu, B.S. Li, H. Yi, Y.K. Fu, L. Li, Z.H. Wang, *Chem. Eng. J.* **383** (2020).
- [89] S. Chen, H. Wang, Z. Kang, S. Jin, X. Zhang, X. Zheng, Z. Qi, J. Zhu, B. Pan, Y. Xie, *Nat. Commun.* **10** (2019) 788.
- [90] Z. Chen, K. Mou, X. Wang, L. Liu, *Angew. Chem. Int. Ed.* **57** (2018) 12790–12794.
- [91] P. Lamagni, M. Miola, J. Catalano, M.S. Hvilsted, M.A.H. Mamakheh, M. Christensen, M.R. Madsen, H.S. Jeppesen, X.M. Hu, K. Daasbjerg, T. Skrydstrup, N. Lock, *Adv. Funct. Mater.* **30** (2020).
- [92] Y.-R. Wang, R.-X. Yang, Y. Chen, G.-K. Gao, Y.-J. Wang, S.-L. Li, Y.-Q. Lan, *Sci. Bull.* **65** (2020) 1635–1642.
- [93] B. Qiao, A. Wang, X. Yang, L.F. Allard, Z. Jiang, Y. Cui, J. Liu, J. Li, T. Zhang, *Nat. Chem.* **3** (2011) 634–641.
- [94] S. Verma, B. Kim, H.-R.M. Jhong, S. Ma, P.J.A. Kenis, *ChemSusChem* **9** (2016) 1972–1979.
- [95] Xuhai Liu, Shengli Zhang, Shiyi Guo, Bo Cai, S. A. Yang, Fukai Shan, Martin Pumera, Haibo Zeng, *Chem. Soc. Rev.*, **49**.
- [96] F. Li, G.H. Gu, C. Choi, P. Kolla, S. Hong, T.-S. Wu, Y.-L. Soo, J. Masa, S. Mukerjee, Y. Jung, J. Qiu, Z. Sun, *Appl. Catal. B* **277** (2020).
- [97] S. Chen, D. Huang, P. Xu, X. Gong, W. Xue, L. Lei, R. Deng, J. Li, Z. Li, *ACS Catal.* **10** (2019) 1024–1059.
- [98] Y. Yang, C. Zhang, D.L. Huang, G.M. Zeng, J.H. Huang, C. Lai, C.Y. Zhou, W.J. Wang, H. Guo, W.J. Xue, R. Deng, M. Cheng, W.P. Xiong, *Appl. Catal. B* **245** (2019) 87–99.
- [99] Y. Yang, Z.T. Zeng, G.M. Zeng, D.L. Huang, R. Xiao, C. Zhang, C.Y. Zhou, W.P. Xiong, W.J. Wang, M. Cheng, W.J. Xue, H. Guo, X. Tang, D.H. He, *Appl. Catal. B* **258** (2019).
- [100] W. Wang, Z. Zeng, G. Zeng, C. Zhang, R. Xiao, C. Zhou, W. Xiong, Y. Yang, L. Lei, Y. Liu, *Chem. Eng. J.* **378** (2019) 122132.
- [101] Z. Wang, M. Chen, D. Huang, G. Zeng, P. Xu, C. Zhou, C. Lai, H. Wang, M. Cheng, W. Wang, *Chem. Eng. J.* **374** (2019) 1025–1045.
- [102] C. Zhou, G. Zeng, D. Huang, Y. Luo, M. Cheng, Y. Liu, W. Xiong, Y. Yang, B. Song, W. Wang, B. Shao, Z. Li, J. Hazard. Mater. **386** (2019) 121947.
- [103] G. Wang, Q. Sun, Y. Liu, B. Huang, Y. Dai, X. Zhang, X. Qin, *Chem.-Eur. J.* **21** (2015) 2364–2367.
- [104] Y. Yang, X. Li, C. Zhou, W. Xiong, G. Zeng, D. Huang, C. Zhang, W. Wang, B. Song, X. Tang, X. Li, H. Guo, *Water Res.* **184** (2020) 116200.
- [105] C. Zhou, P. Xu, C. Lai, C. Zhang, G. Zeng, D. Huang, M. Cheng, L. Hu, W. Xiong, X. Wen, L. Qin, J. Yuan, W. Wang, *Chem. Eng. J.* **359** (2019) 186–196.
- [106] H. Luo, Z. Zeng, G. Zeng, C. Zhang, R. Xiao, D. Huang, C. Lai, M. Cheng, W. Wang, W. Xiong, *Chem. Eng. J.* **(2019)** 123196.
- [107] Z. Huang, Z. Zeng, Z. Song, A. Chen, G. Zeng, R. Xiao, K. He, L. Yuan, H. Li, G. Chen, J. Hazard. Mater. **383** (2020) 121153.

- [108] G. Wang, Y. Liu, B. Huang, X. Qin, X. Zhang, Y. Dai, *Dalton Trans.* 44 (2015) 16238–16241.
- [109] Y. Yang, G. Zeng, D. Huang, C. Zhang, D. He, C. Zhou, W. Wang, W. Xiong, X. Li, B. Li, W. Dong, Y. Zhou, *Appl. Catal. B* 272 (2020).
- [110] K. Xu, L. Wang, X. Xu, S.X. Dou, W. Hao, Y. Du, *Energy Storage Mater.* 19 (2019) 446–463.
- [111] Y. Li, Y. Xu, W. Yang, W. Shen, H. Xue, H. Pang, *Small* 14 (2018) e1704435.
- [112] X. Li, S. Zheng, L. Jin, Y. Li, P. Geng, H. Xue, H. Pang, Q. Xu, *Adv. Energy Mater.* 8 (2018) 1800716.
- [113] A. Thirumurugan, W. Li, A.K. Cheetham, *Dalton Trans.* 41 (2012) 4126–4134.
- [114] P. Mei, L. Wei-Ming, Y. Shao-Yun, S. Si-Si, S. Cheng-Yong, *Chem. Rev.* 118 (2018) acs.chemrev.8b00222.
- [115] X. Zhou, Z. Zeng, G. Zeng, C. Lai, R. Xiao, S. Liu, D. Huang, L. Qin, X. Liu, B. Li, H. Yi, Y. Fu, L. Li, M. Zhang, Z. Wang, *Chem. Eng. J.* 401 (2020).
- [116] B. Zhou, W. Li, J. Zhang, *J. Phys. Chem. C* 121 (2017).
- [117] H. Ouyang, N. Chen, G. Chang, X. Zhao, Y. Sun, S. Chen, H. Zhang, D. Yang, *Angew. Chem. Int. Ed.* 57 (2018) 13197–13201.
- [118] M. Köppen, V. Meyer, J. Ångström, A.K. Inge, N. Stock, *Cryst. Growth Des.* 18 (2018) 4060–4067.
- [119] Y. Bai, Y. Dou, L.H. Xie, W. Rutledge, J.R. Li, H.C. Zhou, *Chem. Soc. Rev.* 45 (2016) 2327–2367.
- [120] T. Tsuruoka, S. Furukawa, Y. Takashima, K. Yoshida, S. Isoda, S. Kitagawa, *Angew. Chem. Int. Ed.* 48 (2009) 4739–4743.
- [121] D. Freudenmann, S. Wolf, M. Wolff, C. Feldmann, *Angew. Chem. Int. Ed.* 50 (2011) 11050–11060.
- [122] A. Pichon, A. Lazuen-Garay, S.L. James, *Cryst. Eng. Comm.* 8 (2006).
- [123] Z. Hu, I. Castano, S. Wang, Y. Wang, Y. Peng, Y. Qian, C. Chi, X. Wang, D. Zhao, *Cryst. Growth Des.* 16 (2016) 2295–2301.
- [124] P. Li, F.-F. Cheng, W.-W. Xiong, Q. Zhang, *Inorg. Chem. Front.* 5 (2018) 2693–2708.
- [125] S. Kumar, S. Jain, M. Nehra, N. Dilbaghi, G. Marrazza, K.-H. Kim, *Coord. Chem. Rev.* 420 (2020).
- [126] Y. Wang, S. Takki, O. Cheung, H. Xu, W. Wan, L. Ohrstrom, A.K. Inge, *Chem. Commun. (Camb.)* 53 (2017) 7018–7021.
- [127] C. Volkringer, D. Popov, T. Loiseau, N. Guillou, G. Ferey, M. Haouas, F. Taulelle, C. Mellot-Draznieks, M. Burghammer, C. Riekel, *Nat. Mater.* 6 (2007) 760–764.
- [128] G. Férey, C. Mellot-Draznieks, C. Serre, F. Millange, J. Dutour, S. Surblé, I. Margiolaki, *Science* 309 (2005) 2040–2042.
- [129] J.L. Mancuso, A.M. Mroz, K.N. Le, C.H. Hendon, *Chem. Rev.* 120 (2020) 8641–8715.
- [130] X. Chen, Y. Cao, H. Zhang, Y. Chen, X. Chen, X. Chai, *J. Solid State Chem.* 181 (2008) 1133–1140.
- [131] X. Yu, H. Zhang, Y. Cao, Z. Hu, Y. Chen, Z. Wang, *J. Solid State Chem.* 179 (2006) 3095–3100.
- [132] A. Thirumurugan, J.-C. Tan, A.K. Cheetham, *Cryst. Growth Des.* 10 (2010) 1736–1741.
- [133] A.C. Wibowo, M.D. Smith, H.-C. zur Loyer, *Cryst. Eng. Comm.* 13 (2011) 426–429.
- [134] X.-X. Xie, Y.-C. Yang, B.-H. Dou, Z.-F. Li, G. Li, *Coord. Chem. Rev.* 403 (2020).
- [135] G.E. Decker, G.R. Lorzing, M.M. Deegan, E.D. Bloch, *J. Mater. Chem. A* 8 (2020) 4217–4229.
- [136] Z. Yin, S. Wan, J. Yang, M. Kurmoo, M.-H. Zeng, *Coord. Chem. Rev.* 378 (2019) 500–512.
- [137] Z. Wang, S.M. Cohen, *J. Am. Chem. Soc.* 129 (2007) 12368–12369.
- [138] J. Della Rocca, D. Liu, W. Lin, *Acc. Chem. Res.* 44 (2011) 957–968.
- [139] Q. Qiu, H. Chen, Y. Wang, Y. Ying, *Coord. Chem. Rev.* 387 (2019) 60–78.
- [140] Y. Sun, L. Zheng, Y. Yang, X. Qian, T. Fu, X. Li, Z. Yang, H. Yan, C. Cui, W. Tan, *Nanomicro Lett.* 12 (2020).
- [141] X. Zhang, S. Yin, S. Wu, W. Dai, W. Li, X. Zhou, *Prog. Chem.* 20 (2008) 878–886.
- [142] S.M.F. Vilela, T. Devic, A. Varez, F. Salles, P. Horcajada, *Dalton Trans.* 48 (2019) 11181–11185.
- [143] S.M.F. Vilela, A.A. Babaryk, R. Jaballí, F. Salles, M.E.G. Mosquera, Z. Elaoud, S. Van Cleuvenbergen, T. Verbiest, P. Horcajada, *Eur. J. Inorg. Chem.* 2018 (2018) 2437–2443.
- [144] C. Liang, H.-Y. Niu, H. Guo, C.-G. Niu, Y.-Y. Yang, H.-Y. Liu, W.-W. Tang, H.-P. Feng, *Chem. Eng. J.* 406 (2021) 126868.
- [145] Y. He, Z. Wang, H. Wang, Z. Wang, G. Zeng, P. Xu, D. Huang, M. Chen, B. Song, H. Qin, Y. Zhao, *Coord. Chem. Rev.* 429 (2021) 213618.
- [146] Z. Xie, W. Xu, X. Cui, Y. Wang, *ChemSusChem* 10 (2017) 1645–1663.